https://doi.org/10.5194/essd-2019-255
Preprint. Discussion started: 20 March 2020
© Author(s) 2020. CC BY 4.0 License.

Open Access Earth System Science Data Discussions

Heat stored in the Earth system: Where does the energy go?

The GCOS Earth heat inventory team

Karina von Schuckmann[1], Lijing Cheng[2], Matthew D. Palmer[3], Caterina Tassone[4], Valentin Aich[4], Susheel Adusumilli[5], Hugo Beltrami[6], Tim Boyer[7], Francisco José Cuesta-Valero[6], Damien Desbruyères[8], Catia Domingues[9,10], Almudena García-García[6], Pierre Gentine[11], John Gilson[12], Maximilian Gorfer[13], Leopold Haimberger[14], Masayoshi Ishii[15], Gregory C. Johnson[16], Rachel Killick[3], Brian A. King[9], Gottfried Kirchengast[13], Nicolas Kolodziejczyk[17], John Lyman[15], Ben Marzeion[18], Michael Mayer[14], Maeva Monier[19], Didier Paolo Monselesan[20], Sarah Purkey[5], Dean Roemmich[5], Axel Schweiger[21], Sonia I. Seneviratne[22], Andrew Shepherd[23], Donald A. Slater[5], Andrea K. Steiner[13], Fiammetta Straneo[5], Mary-Louise Timmermanns[24], Susan E. Wijffels[20,25]

[1]Mercator Ocean International, France
[2]Institute of Atmospheric Physics, Chinese Academy of Sciences, China
[3]Met Office Hadley Centre, UK
[4]WMO/GCOS, Switzerland
[5]Scripps Institution of Oceanography, UCSD, USA
[6]Climate and Atmospheric Sciences Institute, and Environmental Sciences Program, St. Francis Xavier University, Canada
[7]NOAA's National Centers for Environmental Information
[8]University of Brest, CNRS, IRD, Ifremer, IUEM, France.
[9]National Oceanographic Centre, UK
[10]ARC Centre of Excellence for Climate Extremes, University of Tasmania, Hobart, Tasmania, Australia
[11]Earth and Environmental Engineering in the School of Engineering and Applied Sciences, Columbia University, USA
[12]University of California, USA
[13]Wegener Center for Climate and Global Change, University of Graz, Austria
[14]Institute of Meteorology and Geophysics, University of Vienna, Austria
[15]Department of Atmosphere, Ocean and Earth System Modeling Research, Meteorological Research Institute, Japan
[16]NOAA, Pacific Marine Environmental Laboratory, USA
[17] Ifremer, University of Brest, CNRS, IRD, Laboratoire d'Océanographie Physique et Spatiale, IUEM, France
[18]Institute of Geography, University of Bremen, Bremen, Germany
[19]CELAD/Mercator Ocean International, France
[20]CSIRO Oceans and Atmosphere, Hobart, Tasmania, Australia
[21]Applied Physics Laboratory, University of Washington, Seattle, USA
[22]Institute for Atmospheric and Climate Science, ETH, Switzerland
[23]Center for Polar Observation and Modeling, University of Leeds, Leeds, UK
[24]Department of Geology and Geophysics, Yale University, New Haven, USA
[25]Woods Hole Oceanographic Institution, Massachusetts, United States

Correspondence to: Karina von Schuckmann (karina.von.schuckmann@mercator-ocean.fr)

https://doi.org/10.5194/essd-2019-255
Preprint. Discussion started: 20 March 2020
© Author(s) 2020. CC BY 4.0 License.

Open Access Earth System Science Data Discussions

Abstract

Human-induced atmospheric composition changes cause a radiative imbalance at the top-of-atmosphere which is driving global warming. This Earth Energy Imbalance (EEI) is a fundamental metric of climate change. Understanding the heat gain of the Earth system from this accumulated heat – and particularly how much and where the heat is distributed in the Earth system - is fundamental to understanding how this affects warming oceans, atmosphere and land, rising temperatures and sea level, and loss of grounded and floating ice, which are fundamental concerns for society. This study is a Global Climate Observing System (GCOS) concerted international effort to update the Earth heat inventory, and presents an updated international assessment of ocean warming estimates, and new and updated estimates of heat gain in the atmosphere, cryosphere and land over the period 1960-2018. The study obtains a consistent long-term Earth system heat gain over the past 58 years, with a total heat gain of 393 ± 40 ZJ, which is equivalent to a heating rate of 0.42 ± 0.04 Wm^{-2}. The majority of the heat gain (89%) takes place in the global ocean (0-700m: 53%; 700-2000m: 28%; > 2000m: 8%), while it amounts to 6% for the land heat gain, to 4% available for the melting of grounded and floating ice, and to 1% for atmospheric warming. These new estimates indicate a larger contribution of land and ice heat gain (10% in total) compared to previous estimates (7%). There is a regime shift of the Earth heat inventory over the past 2 decades, which appears to be predominantly driven by heat sequestration into the deeper layers of the global ocean, and a doubling of heat gain in the atmosphere. However, a major challenge is to reduce uncertainties in the Earth heat inventory, which can be best achieved through the maintenance of the current global climate observing system, its extension into areas of gaps in the sampling, as well as to establish an international framework for concerted multi-disciplinary research of the Earth heat inventory. Earth heat inventory is published at DKRZ (https://www.dkrz.de/) under the doi: https://doi.org/10.26050/WDCC/GCOS_EHI_EXP (von Schuckmann et al., 2020).

Introduction

The state, variability and change of Earth's climate are to a large extent driven by the energy transfer between the different components of the Earth system (Hansen, 2005; Hansen et al., 2011) (Hansen et al., 2005). Energy flows alter clouds, and weather and internal climate modes can temporarily alter the energy balance for periods of sub-monthly to several decades. The most practical way to monitor climate state, variability and change is to continually assess the energy, mainly in the form of heat, in the Earth system (Hansen et al., 2011). All energy entering or leaving the Earth climate system does so in the form of radiation at the top-of-the-atmosphere (TOA, Loeb et al., 2012). The difference between incoming solar radiation and outgoing radiation, which is the sum of the reflected shortwave radiation and emitted longwave radiation, determines the net radiative flux at TOA. Changes of this global radiation balance at TOA - the so-called Earth Energy Imbalance (EEI) - determines the temporal evolution of Earth climate: If the imbalance is positive

https://doi.org/10.5194/essd-2019-255
Preprint. Discussion started: 20 March 2020
© Author(s) 2020. CC BY 4.0 License.

(i.e. more energy coming in than going out), energy in the form of heat is accumulated in the climate system resulting in global warming, or cooling if the EEI is negative. The various facets and impacts of observed climate change arise due to the EEI, which thus represents a crucial measure of the rate of climate change (von Schuckmann et al., 2016). In particular, EEI is less subject to decadal variations associated with internal climate variability than global surface temperature and therefore represents a more robust measure of the rate of climate change that is more indicative of the time-evolution of the Earth's radiative forcing.

In the context of climate change, anthropogenic radiative forcing of the climate system has given rise to an Earth's energy imbalance, primarily from increases in atmospheric greenhouse gas concentrations (Myhre, G. et al., 2013). The Earth system responds to an imposed radiative forcing through a number of feedbacks, which operate on various different timescales. Conceptually, the relationships between radiative forcing, EEI and surface temperature change can be expressed as (e.g. Gregory and Andrews, 2016):

$$N = F - \alpha T$$

Where N is Earth's energy imbalance (W m^{-2}), F is the radiative forcing (W m^{-2}), T is the global surface temperature anomaly (K) relative to the equilibrium state, and α is the net feedback parameter (W m^{-2} K^{-1}), which represents the combined effect of the various climate feedbacks. Essentially, α can be viewed as a measure of how efficient the system is at restoring radiative equilibrium for a unit surface temperature rise. Thus, N, represents the difference between the applied radiative forcing and Earth's radiative response through climate feedbacks associated with surface temperature rise. Observation-based estimates of N are crucial both to our understanding of past climate change and for refining projections of future climate change (e.g. Gregory and Andrews, 2016; Kuhlbrodt and Gregory, 2012). The long atmospheric lifetime of carbon dioxide means that F, N and T will remain positive for centuries, even with substantial reductions in greenhouse gas emissions and lead to substantial committed sea-level rise (Nauels et al., 2017; Palmer et al., 2018).

Time-scales of the Earth climate response to perturbations of the equilibrium Earth energy balance at TOA are driven by a combination of climate forcing and the planet's thermal inertia: The Earth system tries to restore radiative equilibrium through increased thermal radiation to space via the Planck response, but a number of additional Earth system feedbacks also influence the planetary radiative response (e.g. Lembo et al., 2019; Myhre et al., 2013). Time-scales of warming or cooling of the climate depend on the imposed radiative forcing, the evolution of climate and Earth system feedbacks with ocean and cryosphere in particular leading to substantial "thermal inertia" (e.g. Clark et al., 2016; Marshall et al., 2015). Consequently, it requires centuries for Earth's surface temperature to respond fully to a climate forcing. In addition to forcing of the climate system, perturbations to the energy balance at TOA arise from internal climate variations. For example, at time scales from interannual to decadal periods, the phase of the El Niño Southern Oscillation

https://doi.org/10.5194/essd-2019-255
Preprint. Discussion started: 20 March 2020
© Author(s) 2020. CC BY 4.0 License.

127 contributes to both positive or negative variations in EEI (e.g. Loeb et al., 2012). At multi-decadal
128 and longer time scales, systematic changes in ocean circulation can significantly alter the EEI as
129 well (Baggenstos et al., 2019).
130
131 Contemporary estimates of the magnitude of the Earth's energy imbalance range between about
132 0.4-1.0 W m^{-2} (depending on estimate method and period, see Table 1), and are directly attributable
133 to increases in carbon dioxide and other greenhouse gases in the atmosphere from human activities
134 (Ciais et al., 2013). Since the period of industrialization, the EEI has become increasingly
135 dominated by the emissions of radiatively active greenhouse gases, which perturb the planetary
136 radiation budget and result in a positive EEI. As a consequence, excess heat is accumulated in the
137 Earth system, which is driving global warming (Hansen et al., 2005; 2011). The majority (about
138 90%) of this positive EEI is stored in the ocean and can be estimated through the evaluation of
139 ocean heat content (OHC). According to previous estimates, a small proportion (~3%) contributes
140 to the melting of arctic sea ice and land ice (glaciers, Greenland and Antarctica). Another 4% goes
141 into heating of the land and atmosphere (Rhein et al., 2013).
142
143 Knowing where and how much heat is stored in the different Earth system components from a
144 positive EEI, and quantifying the Earth heat inventory is of fundamental importance to unravel the
145 current status of climate change, as well as to better understand and predict the implications of
146 climate change, and to design the optimal observing networks for monitoring the Earth heat
147 inventory. Moreover, quantifying this energy gain is essential for understanding the response of
148 the climate system to radiative forcing, and hence to reduce uncertainties in climate predictions.
149 The rate of OHC as a key component for the quantification of the EEI, and the observed surface
150 warming has been used to estimate the equilibrium climate sensitivity (e.g. Knutti and Rugenstein,
151 2015). However, further insight into the Earth energy inventory, particularly to further unravel on
152 where the heat is going can have implications on the understanding of the transient climate
153 responses to climate change, and consequently reduces uncertainties in climate predictions.
154
155 There are different approaches to estimate the absolute value of the EEI and its changes over time
156 (see Table 1). In this paper, we focus on the inventory of heat stored in the Earth system. The first
157 four sections will introduce the current status of estimate of heat storage change in the ocean,
158 atmosphere, land and cryosphere, respectively. Uncertainties, current achieved accuracy,
159 challenges, and recommendations for future improved estimates are discussed for each Earth
160 system component. In the last chapter, an update of the Earth heat inventory is established based
161 on the results of sections 1-4.
162
163
164
165

https://doi.org/10.5194/essd-2019-255
Preprint. Discussion started: 20 March 2020
© Author(s) 2020. CC BY 4.0 License.

Period	EEI estimate (W/m^2)	Reference
1960-2015	0.4 ± 0.1	Cheng et al., 2017
1993-2008	0.8 - 0.9 ± 0.1	Trenberth et al., 2011; Trenberth and Fasullo, 2011; Hansen et al., 2011; Balmaseda et al., 2013b
1993-2008	0.57 ± 0.1	Hansen et al., 2001
1993-2015	0.4 ± 0.1	von Schuckmann et al., 2017
2001-2010	0.50 ± 0.43	Loeb et al., 2012
2001-2011	0.5-1	Trenberth et al., 2014
2005-2010	0.58 ± 0.15	Hansen et al., 2011
2005-2013	0.7 ± 0.1	Dieng et al., 2017
2005-2015	0.7-0.9 ± 0.1	Trenberth et al., 2016, Johnson et al., 2016
2005-2016	0.7± 0.1	von Schuckmann et al., 2018

Table 1: *Estimate of the Earth Energy Imbalance as published in recent scientific literature, and based on estimates using satellite derived estimates of net flux at the Top Of the Atmosphere (TOA), and the rate of change of ocean heat content.*

1. Heat stored in the oceans

The storage of heat in the ocean leads to ocean warming and is a major contributor to sea-level rise through thermal expansion (WCRP, 2018)(WCRP, 2018). Ocean warming is altering ocean stratification and ocean mixing processes (Capotondi et al., 2012), affects ocean currents (Hoegh-Guldberg, O., 2018; Rhein et al., 2018; Yang et al., 2016), impacts tropical cyclones (Hoegh-Guldberg, O., 2018; Trenberth et al., 2018; Woollings et al., 2012; Yang et al., 2016) and is a major player in ocean deoxygenation processes (Breitburg et al., 2018) and carbon sequestration

https://doi.org/10.5194/essd-2019-255
Preprint. Discussion started: 20 March 2020
© Author(s) 2020. CC BY 4.0 License.

into the ocean (Bopp et al., 2013; Frölicher et al., 2018). Together with ocean acidification and deoxygenation, ocean warming can lead to dramatic changes in ecosystems, biodiversity, population extinctions, coral bleaching and infectious disease, change in behavior (including reproduction), as well as redistribution of habitat (e.g. García Molinos et al., 2016; Gattuso et al., 2015; Ramírez et al., 2017). Implications of ocean warming are also widespread across Earth's cryosphere (e.g. Mayer et al., 2019; Polyakov et al., 2017; Serreze and Barry, 2011; Shi et al., 2018), and have in turn impacted the ocean itself (e.g. Jacobs et al., 2002). Examples include the imbalance of floating ice shelves and marine terminating glaciers from basal ice melt (Straneo and Cenedese, 2015; Wilson et al., 2017); the retreat and speedup of ice sheet outlet glaciers in Greenland (Straneo et al., 2019b) and in Antarctica (Shepherd et al., 2018a) and of tidewater glaciers in South America and in the High Arctic (e.g. Gardner et al., 2013), as well as thinning of floating ice shelves in the Antarctic Peninsula (e.g. Pritchard et al., 2012).

Opportunities, but also challenges of Ocean Heat Content (OHC) estimates depend on the availability of in situ subsurface temperature measurements, particularly for global-scale evaluations. Early subsurface ocean temperature measurements before 1900 had been obtained from ship-board instrumentation during two large expeditions, i.e. one Captain James Cook's expedition in the Southern Ocean (1772–1775), and the global-scale Challenger expedition (1873–1876) (e.g. Roemmich and Gilson, 2009). Since then and up to the mid-1960s, subsurface temperature measurements relied on so called ship-board Nansen-Bottle and mechanical bathythermograph (MBT) instruments (e.g. Abraham et al., 2013), only allowing limited global coverage and data quality. The inventions of the conductivity-temperature-depth (CTD) instruments in the mid-50s and the Expendable Bathythermograph Observing (XBT) system about ten years later increased the oceanographic capabilities for widespread and accurate (in the case of the CTD) measurements of in situ subsurface water temperature (e.g. Abraham et al., 2013; Goni et al., 2019).

With the implementation of several national and international programs, and the implementation of the fixed moorings in the tropical ocean in the 1980s, the Global Ocean Observing System (GOOS, https://www.goosocean.org/) started to grow. Particularly the global World Ocean Circulation program (WOCE) during the 1990s obtained a global baseline survey of the oceans from top-to-bottom (King et al., 2001). However, measurements were still limited to fixed point measurement platforms, major shipping routes and Naval and research vessel cruise tracks, leaving large parts of the ocean under-sampled. In addition, detected instrumental biases in both MBTs and XBTs further challenged the global scale ocean heat content estimate (Ciais et al., 2013; Rhein et al, 2013), but significant progress has been made recently to correct the biases and provide high-quality data for climate research (Boyer et al., 2016; Cheng et al., 2016; Goni et al., 2019). Satellite altimeter measurements of sea surface height began in 1992, and are used to complement in situ derived ocean heat content estimates, either for validation purposes (Cabanes et al., 2013), or to complement the development of global gridded ocean temperature fields (e.g. (Guinehut et al.,

https://doi.org/10.5194/essd-2019-255
Preprint. Discussion started: 20 March 2020
© Author(s) 2020. CC BY 4.0 License.


2012; Willis et al., 2004). Indirect estimates of OHC from remote sensing through the global sea level budget became possible with the satellite-derived ocean mass information in 2002 ((Dieng et al., 2017; Llovel et al., 2014; Loeb et al., 2012; Meyssignac et al., 2019; von Schuckmann et al., 2014).

After the Oceanobs conference in 1999, the international Argo profiling float program was launched with first Argo float deployments in the same year (Riser et al., 2016; Roemmich and Gilson, 2009). By the end of 2006, Argo sampling had reached its initial target of data sampling roughly every 3 degrees between 60°S-60°N. However, due to technical evolution, only 40% of Argo floats provided measurements down to 2000 m depth in the year 2005, but that percentage increased to 60% in 2010 (von Schuckmann and Le Traon, 2011). The starting point of a 'best estimate' for near-global-scale (60°S-60°N) OHC is either defined in 2005 (e.g. von Schuckmann and Le Traon, 2011), or in 2006 (e.g. (Wijffels et al., 2016). The improvement for Argo-based estimates of OHC is tremendous, and has led to major advancements in climate science, particularly on the discussion of the EEI (e.g. Hansen et al., 2011; Johnson et al., 2018; Loeb et al., 2012; von Schuckmann et al., 2016; Trenberth and Fasullo, 2010). The near-global coverage of the Argo network also provides an excellent test bed for the long-term OHC reconstruction extending back well before the Argo period (Cheng et al., 2017). Moreover, these evaluations allow further observing system recommendations for global climate studies, i.e. gaps in the deep ocean layers below 2000m depth, in marginal seas, in shelf areas and in the polar regions (e.g. von Schuckmann et al., 2016), and their implementations are underway (e.g., Johnson et al., 2019 for deep Argo).

Different research groups have developed gridded products of subsurface temperature fields for the global ocean using statistical models (e.g. Good et al., 2013; Ishii et al., 2017; Levitus et al., 2012) or combined observations with additional information from climate models (Cheng et al., 2017). An exhaustive list of the pre-Argo products can be found in for example Abraham et al., 2013; Boyer et al., 2016; Group, 2018; Meyssignac et al., 2019. Additionally, specific Argo-based products are listed on the Argo webpage (http://www.argo.ucsd.edu/). Although all products rely more or less on the same database, near-global OHC estimates show some discrepancies which result from the different statistical treatments of data gaps, the choice of the climatology and the approach used to account for the MBT and XBT instrumental biases (Boyer et al., 2016). Although reduced, the Argo-based products also show differences, which are discussed to result from different treatments of currently under-sampled regions (e.g. von Schuckmann et al., 2016). Ocean reanalysis systems have been also used to deliver estimates of near-global OHC (e.g; (Meyssignac et al., 2019; von Schuckmann et al., 2018), and their international assessments show increased discrepancies with decreasing in situ data availability for the assimilation (e.g. Palmer et al., 2017; Storto et al., 2018) Climate models have also been used to study global and regional ocean heat changes and the associated mechanisms, with observational datasets providing valuable benchmarks for model evaluation (Cheng et al., 2016, 2019; Gleckler et al., 2016).

https://doi.org/10.5194/essd-2019-255
Preprint. Discussion started: 20 March 2020
© Author(s) 2020. CC BY 4.0 License.

International near-global OHC assessments have been performed previously (e.g. Abraham et al., 2013; Boyer et al., 2016; Meyssignac et al., 2019; WCRP, 2018). These assessments are challenging, as most of the gridded temperature fields are research products, and only few are distributed and regularly updated operationally. The initiative relies on the availability of data products, their temporal extensions, and direct interactions with the different research groups. As a consequence, a complete and holistic view on all available international temperature products can be only achieved through a concerted international effort, and over time. In this study, we did not achieve a holistic view of all available products, but we assay a starting point for future international regular assessments of near-global OHC. For the first time, we propose an international ensemble mean and standard deviation of near-global OHC (Fig. 1) which is then used to build an Earth climate system energy inventory (section 5). However, future evolution of this initiative is needed to include all missing in situ-based products, ocean reanalyses, as well as satellite-based indirect estimates.

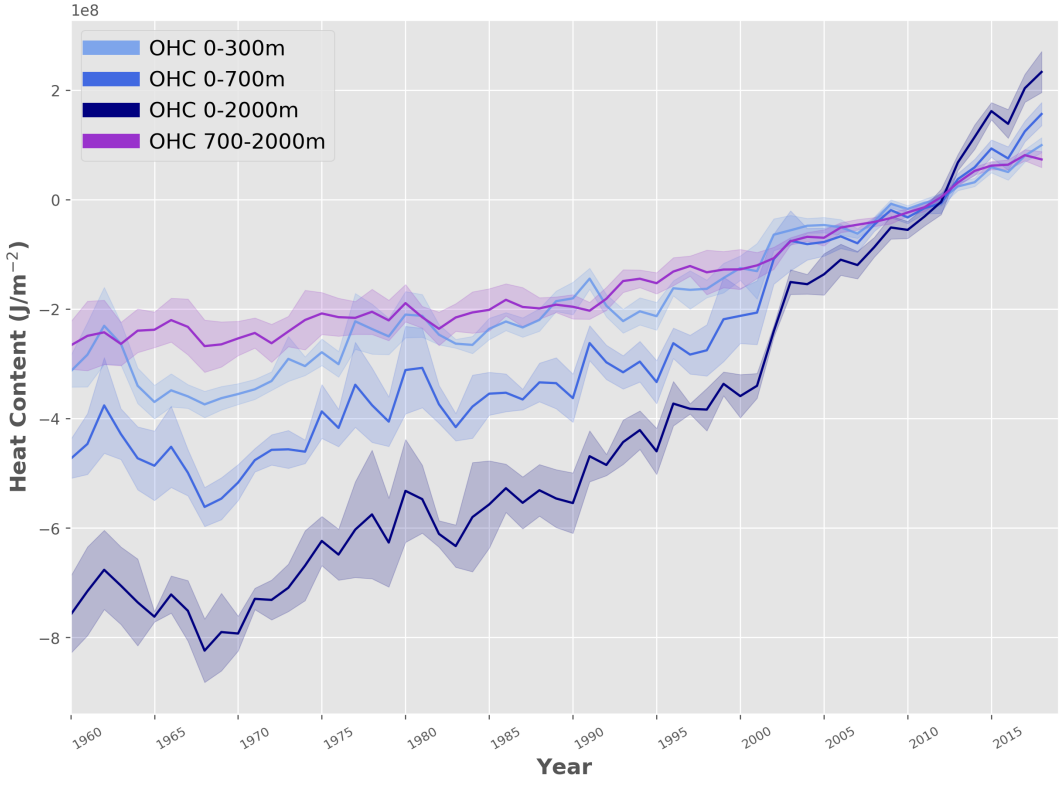

Figure 1: *Ensemble mean time series and ensemble standard deviation (2-sigma, shaded) of global ocean heat content anomalies relative to the 2005-2018 climatology for the 0-300m (light blue), 0-700m (blue), 0-2000m (dark blue) and 700-2000m depth layer. The ensemble mean is an outcome of an international assessment initiative, and all products used are referenced in the Figure caption of Fig. 2. The trends over*

https://doi.org/10.5194/essd-2019-255
Preprint. Discussion started: 20 March 2020
© Author(s) 2020. CC BY 4.0 License.

the period 1960-2018 (1993-2018; 2005-2018) amount to 0.2 (0.4; 0.4) W/m^2 for 0-300m; 0.3 (0.6; 0.6) W/m^2 for 0-700m; 0.5 (0.9; 0.9) W/m^2 for 0-2000m; 0.2 (0.3; 0.4) W/m^2 for 700-2000m depth layers, respectively. All trends range between about ±0.1 W/m^2. Note that values are given for the ocean surface.

Products used for this assessment are referenced in the caption of Fig. 2. Estimates of OHC have been provided by the different research groups under homogeneous criteria. All estimates use a coherent ocean volume limited by the 300m isobath of each product. All estimates are limited to 60°S-60°N (called 'near-global' hereinafter), and only annual averages have been used. The assessment is based on three distinct periods to account for the evolution of the observing system, i.e. 1960-2018 (i.e. 'historical'), 1993-2018 (i.e. 'altimeter era') and 2005-2018 (i.e. 'Argo-era'). All time series reach the end 2018 – which was one of the principal limitations for the inclusion of some products. Our final estimates of OHC at upper 2000m in different periods are the ensemble average of all products, with the uncertainty range defined by the standard deviation (2-sigma) of the corresponding estimates used.

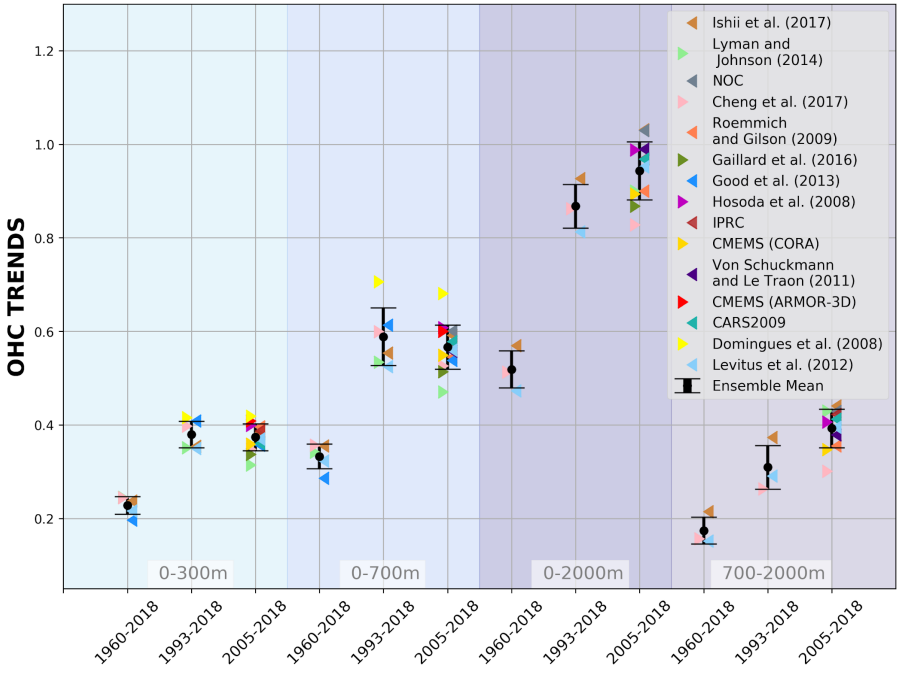

Figure 2: *Trends of global ocean heat content as derived from different temperature products (colors). References are given in the figure legend, except for IPRC (http://apdrc.soest.hawaii.edu/projects/Argo/), CMEMS (CORA & ARMOR-3D, http://marine.copernicus.eu/science-learning/ocean-monitoring-*

https://doi.org/10.5194/essd-2019-255
Preprint. Discussion started: 20 March 2020
© Author(s) 2020. CC BY 4.0 License.

indicators)CAR2009 (http://www.marine.csiro.au/~dunn/cars2009/) and NOC (National Oceanographic Institution, Desbruyères et al., 2016*. The ensemble mean and standard deviation (2-sigma) is given in black, respectively. The shaded areas show trends from different depth layer integrations, i.e. 0-300m (light turquoise), 0-700m (light blue), 0-2000m (purple) and 700-2000m (light purple). For each integration depth layers, trends are evaluated over the three study periods, i.e. historical (1960-2018), altimeter era (1993-2018) and Argo era (2005-2018). See text for more details on the international assessment criteria. Note that values are given for the ocean surface.*

The first and principal result of the assessment (Fig. 1) is an overall increase of the trend for the more recent two study periods e.g., the altimeter era (1993-2018) and Argo era (2005-2018) relative to the historical era (1960-2018). The trend values are all given in the caption of Fig. 1. A major part of heat is stored in the upper layers of the ocean (0-300m and 0-700m depth). However, heat storage in the intermediate layer (700-2000m) increases at a comparable rate as reported for the 0-300m depth layer, the rate of change jumps from 0.2 (0.4; 0.4) W/m^2 for 0-300m to 0.5 (0.9; 0.9) W/m^2 for the 0-2000m depth layer over the study periods 1960-2018 (1993-2018; 2005-2018). There is a general agreement between the 15 international OHC estimates (Fig. 2). However, for some periods and depth layers the standard deviation reaches maximal values up to about 0.3 W/m^2. All products agree on the fact that ocean warming rates have increased in the past decades, and doubled since the beginning of the altimeter era (1993-2018 compared with 1960-2018) (Fig. 2). Moreover, there is a clear indication that heat sequestration into the deeper ocean layers took place over the past 6 decades.

For the deep OHC changes below 2000m, we adapted an updated estimate from Purkey and Johnson (2010) (PG10) from 1991 to 2018, which is a constant linear trend estimate (1.15 +/- 0.57 ZJ/year, 0.07 +/- 0.04 W/m^2). Some recent studies strengthened the results in PG10 (Desbruyères et al., 2016; Zanna et al., 2019). Desbruyères et al., (2016) examined the decadal change of the deep and abyssal OHC trends below 2000m in 1990s and 2000s, suggesting that there has not been a significant change in the rate of decadal global deep/abyssal warming from the 1990's to the 2000's and the overall deep ocean warming rate is consistent with PG10. Using a Green Function method, Zanna et al. (2019) reported a deep ocean warming rate of ~0.06 Wm^{-2} during the 2000s, consistent with PG10 used in this study. Zanna et al. (2019) shows a fairly weak global trend during the 1990s, inconsistent with observation-based estimates. This mismatch might come from the misrepresentation of surface-deep connections in ECCO reanalysis data and the use of time-mean Green functions in Zanna et al. (2019). Furthermore, combining hydrographic and deep-Argo floats, a recent study (Johnson et al., 2019) reported an accelerated warming in the South Pacific Ocean in recent years, but a global estimate on the OHC rate change over time is not available yet.

https://doi.org/10.5194/essd-2019-255
Preprint. Discussion started: 20 March 2020
© Author(s) 2020. CC BY 4.0 License.

Before 1990, we assume zero OHC trend below 2000m, following the methodology in IPCC-AR5 (Rhein et al., 2013). The zero-trend assumption is made mainly because there are too few observations before 1990 to make an estimate of OHC change below 2000m. But it is a reasonable assumption because OHC700-2000m warming is fairly weak before 1990 and heat might not have penetrated down to 2000m. Zanna et al. (2019)also shows a near zero OHC trend below 2000m from 1960s to 1980s. The derived time series is for the Earth energy inventory in section 5.

2. Heat available to warm the atmosphere

Warming of the Earth's surface and its atmosphere is one prominent effect of climate change, which directly affects society. Atmospheric observations clearly reveal a warming of the troposphere over the last decades (e.g., Santer et al., 2017; Steiner et al., 2019) and changes in the seasonal cycle (Santer et al., 2018). Changes in atmospheric circulation (e.g., Cohen et al., 2014; Fu et al., 2019) together with thermodynamic changes (e.g., Fischer and Knutti, 2016; Trenberth et al., 2015) will lead to more extreme weather events and increase high impact risks for society (e.g., Coumou et al., 2018; Zscheischler et al., 2018). Therefore, a rigorous assessment of the atmospheric heat content in context with all Earth's climate subsystems is important for a full view on the changing climate system.

The atmosphere transports vast amounts of energy laterally and strong vertical heat fluxes occur at the atmosphere's lower boundary. The pronounced energy and mass exchanges within the atmosphere and with other climate components is a fundamental element of Earth's climate (Peixoto and Oort, 1992). In contrast, long-term heat accumulation in the atmosphere is limited by its small heat capacity (von Schuckmann et al., 2016). In a globally averaged and vertically integrated sense, heat accumulation in the atmosphere arises from a small imbalance between net energy fluxes at the top of the atmosphere (TOA) and the surface (denoted s). The heat budget of the vertically integrated and globally averaged atmosphere (indicated by the global averaging operator <.>) reads as follows:

$$< \frac{\partial AE}{\partial t} > = < Rad_{TOA} > - < F_s > - < F_{snow} > - < F_{PE} >, \qquad (1)$$

where, in vertical pressure (p) coordinates, the vertically integrated atmospheric energy content AE per unit surface area [Jm^{-2}] reads

$$AE = \int_{p_{TOA}}^{p_s} \frac{1}{g}(c_v T + \Phi + L_e q + K)\, dp, \qquad (2)$$

while in mean-sea-level altitude (z) coordinates, used for the observational datasets, it can be written as

$$AE = \int_{z_s}^{z_{TOA}} \rho(c_v T + g(z - z_s) + L_e q + \frac{1}{2}V^2)\, dz. \quad (3)$$

https://doi.org/10.5194/essd-2019-255
Preprint. Discussion started: 20 March 2020
© Author(s) 2020. CC BY 4.0 License.

In Equation 1, AE represents the total atmospheric energy content, Rad_{TOA} the net radiation at top-of-the atmosphere, F_s net surface energy flux defined as the sum of net surface radiation and latent and sensible heat flux, F_{snow} the latent heat flux associated with snowfall (computed as the product of latent heat of fusion and snow fall rate), and F_{PE} is the difference of surface enthalpy fluxes arising from global evaporation and precipitation.

F_{snow} represents a heat flux that is directed in the opposite direction than the associated mass flux: it warms the atmosphere by additional latent heat release and cools the underlying surface. This is analogous to the energetic effect of sea ice export from the Arctic. F_{snow} cools the high latitude ocean with rates up to 5 Wm^{-2}, but its global average value is smaller than 1 Wm^{-2} (Mayer et al., 2017). Snowfall is also an important contributor to the heat and mass budget of ice-sheets and sea ice (see section 4).

F_{PE} represents the net heat flux arising from the different temperatures of rain and evaporated water. This flux can be sizeable regionally, but it is small in a global average sense (warming of the atmosphere ~0.3 Wm^{-2} according to Mayer et al., 2017).

Equations 2 and 3 provide a decomposition of the atmospheric energy content AE, where g is the acceleration of gravity, c_v the specific heat for moist air at constant volume, c_v the specific heat at constant volume, ρ the air density, T is air temperature, ρ the air density, Φ_S the surface geopotential above surface, K kinetic energy, V wind speed, L_e the temperature-dependent effective latent heat of condensation (and vaporization) L_v or sublimation L_s (the latter relevant below 0 °C), and q the specific humidity of the moist air. We neglect atmospheric liquid water droplets and ice particles as separate species, as their amounts and especially their trends are small.

In the AE derivation from the observational datasets based on Equation 3, we accounted for the intrinsic temperature dependence of the latent heat of water vapor by assigning L_e to L_v if ambient temperatures are above 0 °C and to L_s (adding in the latent heat of fusion L_f) if they are below –10 °C, respectively, with a gradual (half-sine weighted) transition over the temperature range between. The reanalysis evaluations, following Equation 2, similarly approximate L_e by using values of L_v, L_s, and L_f, though in slightly differing forms. The resulting differences in AHC anomalies from any of these choices are negligibly small, however, since the latent heat contribution at low temperatures is itself very small.

Similarly, the AE estimations from the observations neglected the kinetic energy term K in Equation 3 (fourth term), while it accounted for the sensible heat energy (sum of the first two terms, internal heat energy and gravity potential energy) and the latent heat energy (third term). This as well leads to negligible differences to the use of Equation 2, since the kinetic energy content and trends at global scale are more than three orders of magnitude smaller than from the sensible heat content.

Turning to the datasets used, atmospheric energy accumulation can be quantified using various data types, as summarized in the following. Atmospheric reanalyses combine observational information from various sources (radiosondes, satellites, weather stations, etc.) and a dynamical model in a statistically optimal way. This data type has reached a high level of maturity, thanks to continuous development work since the early 1990s (e.g., Hersbach et al., 2018). Especially

https://doi.org/10.5194/essd-2019-255
Preprint. Discussion started: 20 March 2020
© Author(s) 2020. CC BY 4.0 License.


reanalysed atmospheric state quantities like temperature, winds, and moisture are considered to be of high quality and suitable for climate studies, although temporal discontinuities introduced from the ever-changing observation system remain a matter of concern (Berrisford et al., 2011; Chiodo and Haimberger, 2010).

Here we use the current generation of atmospheric reanalyses as represented by ECMWF's fifth-generation reanalysis ERA5 (Hersbach et al., 2018, 2019), NASA's Modern-Era Retrospective analysis for Research and Applications version 2 (MERRA2; Gelaro et al., 2017), and JMA's 55-year-long reanalysis JRA55 (Kobayashi et al., 2015). All these are available over 1980 to 2018; the latter is the only one also covering the timeframe 1960 to 1979. We additionally used a different version of JRA55 that assimilates only conventional observations, which away from the surface only leaves radiosondes as data source (JRA55C). The advantage of this product is that it avoids potential spurious jumps associated with satellite changes. Moreover, JRA55C is fully independent of satellite-derived Global Positioning System (GPS) radio occultation (RO) data that are also separately used and described below together with the observational techniques.

The datasets from three different observation techniques have been used for complementary observational estimates of the atmospheric heat content. We use the Wegener Center (WEGC) multi-satellite RO data record, WEGC OPSv5.6 (Angerer et al., 2017), as well as its radiosonde (RS) data record derived from the high-quality Vaisala sondes RS80/RS92/VS41, WEGC Vaisala (Ladstädter et al., 2015). WEGC OPSv5.6 and WEGC Vaisala provide thermodynamic upper air profiles of air temperature, specific humidity, and density from which we locally estimate *AE* according to Equation 3 (Kirchengast et al., 2019). In atmospheric domains not fully covered by the data (e.g., in the lower part of the boundary layer for RO or over the polar latitudes for RS) the profiles are vertically completed by collocated ERA5 information. The local vertical energy content results are then averaged into regional monthly means, which are finally geographically aggregated to global atmospheric heat content (AHC). Applying this estimation approach in the same way to reanalysis profiles sub-sampled at the observation locations accurately leads to the same AHC anomaly time series records as the direct estimation from the full gridded fields based on Equation 2.

The third observation-based AHC dataset derives from a rather approximate estimation approach using the microwave sounding unit (MSU) data records (Mears and Wentz, 2017). Because the very coarse vertical resolution of the brightness temperature measurements from MSU does not enable integration according to Equation 2 or 3, this dataset is derived by replicating the method used in IPCC AR5 WGI Assessment Report 2013 (Rhein, M., Rintoul, S., Aoki, S., Campos, E., Chambers, D., Feely, R., Gulev, S., Johnson, G., Josey, S., Kostianoy, A., Mauritzen, C., Roemmich, D., Talley, L., and Wang, 2013; Chap. 3, Box 3.1 therein). We used the most recent MSU Remote Sensing System (RSS) V4.0 temperature dataset (Mears and Wentz, 2017), however, instead of MSU RSS V3.3 that was used in the IPCC AR5 (Mears and Wentz, 2009a, 2009b; updated to version 3.3). In order to derive global time series of AHC anomalies, the approach simply combines weighted MSU lower tropospheric temperature and lower stratospheric temperature changes (TLT and TLS channels) converted to sensible heat content changes via

https://doi.org/10.5194/essd-2019-255
Preprint. Discussion started: 20 March 2020
© Author(s) 2020. CC BY 4.0 License.

global atmospheric mass, and an assumed fractional increase of latent heat content according to water vapor content increase driven by temperature at a near-Clausius-Clapeyron rate (7.5 %/°C).

Figure 3 shows the resulting global AHC change inventory over 1980 to 2018 in terms of AHC anomalies of all data types (top), mean anomalies and time-average uncertainty estimates including long-term AHC trend estimates (middle), and annual-mean AHC change estimates (bottom). The mean anomaly time series (middle left), preceded by the small JRA-55 anomalies over 1960-1979 is used as part of the overall heat inventory in Section 5 below. Results including MSU in addition are separately shown (right column), since this dataset derives from a fairly approximate estimation as summarized above and hence is given lower confidence than the others deriving from rigorous AHC integration & aggregation. Since it was the only dataset for AHC change estimation in the IPCC AR5 report, bringing it into context is considered relevant, however.

The results clearly show that the AHC trends have intensified from the earlier decades represented by the 1980-2010 trends of near 1.8 TW (consistent with the trend interval used in the IPCC AR5 report). We find the trends about 2.5 times higher over 1993-2018 (about 4.5 TW) and about three times higher in the most recent two decades over 2002-2018 (near 5.3 TW), a period that is already fully covered also by the RO and RS records (which estimate around 6 TW). The year-to-year annual-mean changes in AHC, reaching amplitudes as high as 50 to 100 TW (or 0.1 to 0.2 Wm^{-2}, if normalized to the global surface area), indicate the strong coupling of the atmosphere with the uppermost ocean. This is mainly caused by ENSO interannual variations that lead to substantial reshuffling of heat energy between the atmosphere and the uppermost ocean layer down to about 300 m (Johnson et al., 2019).

https://doi.org/10.5194/essd-2019-255
Preprint. Discussion started: 20 March 2020
© Author(s) 2020. CC BY 4.0 License.

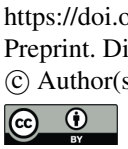

Open Access Earth System Science Data Discussions

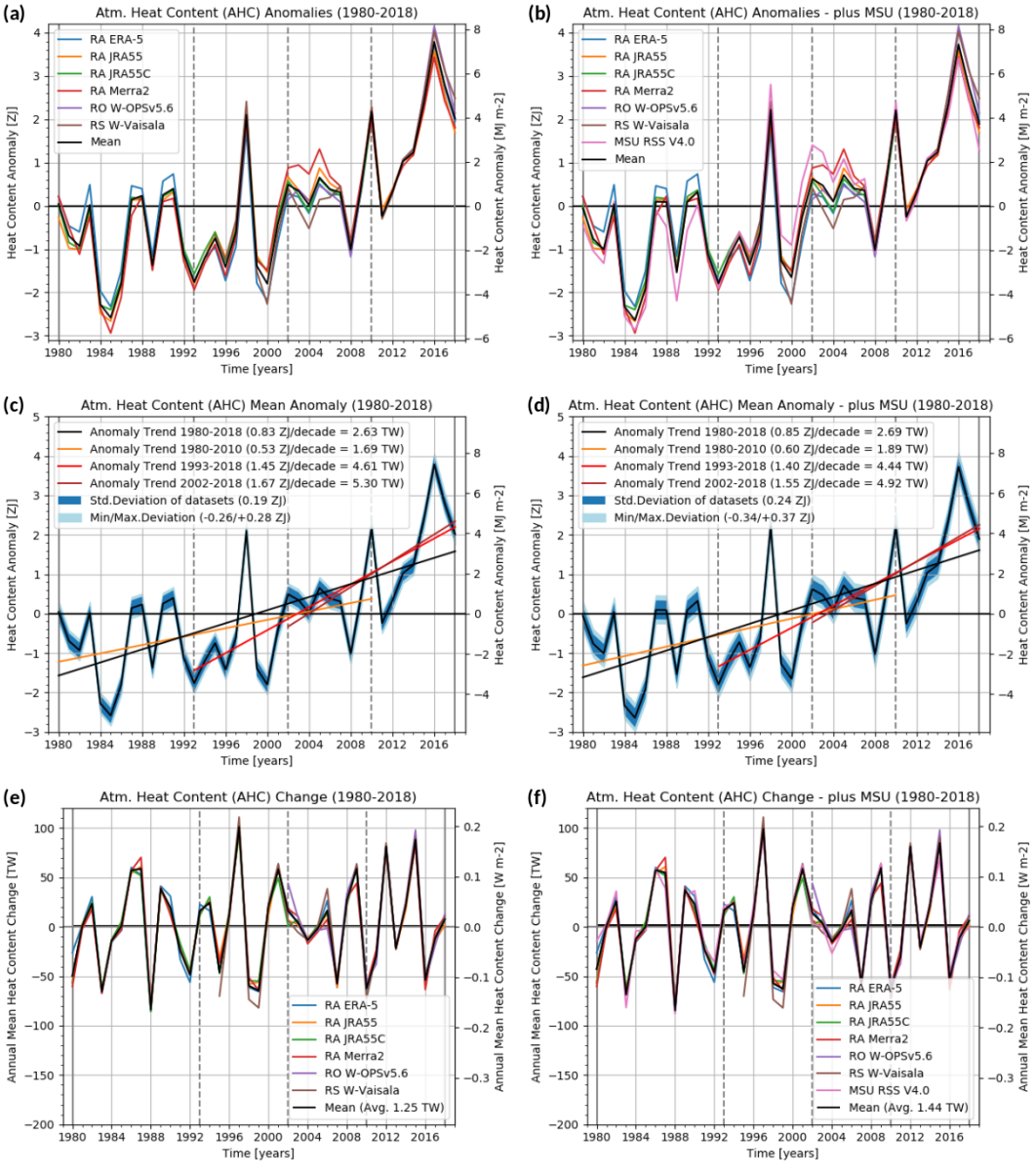

Figure 3: *Annual-mean global AHC anomalies over 1980 to 2018 of four different reanalyses and two (left) or three (right, plus MSU) different observational datasets shown together with their mean (top), the mean AHC anomaly shown together with four representative AHC trends and ensemble spread measures of its underlying datasets (middle), and the annual-mean AHC change shown for each year over 1980 to 2018 for all datasets and their mean (bottom). The in-panel legends identify the individual datasets shown (top and bottom) and the chosen trend periods together with the associated trend values and spread measures (middle), the latter including the time-average standard deviation and minimum/maximum deviations of the individual datasets from the mean.*

https://doi.org/10.5194/essd-2019-255
Preprint. Discussion started: 20 March 2020
© Author(s) 2020. CC BY 4.0 License.


3. Heat available to warm land

The present global energy imbalance due to the release of greenhouse gasses from the combustion of fossil fuels and from land use changes since about 1850 CE (Irving et al., 2019; Loeb et al., 2016) has perturbed the prevailing flow of energy among climate subsystems (Hansen et al., 2011; Lembo et al., 2019; von Schuckmann et al., 2016). Such modifications in the dynamics of the climate system are perceived by society and the ecosystem as climate change. Thus, estimating the energy content of each Earth's climate subsystems is crucial to be able to assess the potential evolution of the climate system.

Although it had been previously estimated that about 93% (Gleckler et al., 2016; Hansen et al., 2011; Levitus et al., 2012) of the global excess energy is absorbed by the ocean and the fraction of energy flowing into the land surface is much smaller, the land component of the Earth's energy budget is important because several land based processes playing a crucial role in the future evolution of climate are sensitive to the magnitude of the available land heat. These radiatively relevant processes include the stability and extent of the continental areas occupied by permafrost soils. Alterations of the thermal conditions at these locations have the potential to release long-term stored CO_2 and CH_4, and may also destabilize the recalcitrant soil carbon (Bailey et al., 2019; Hicks Pries et al., 2017). Both of these processes are potential "tipping points" (Lenton et al., 2019, 2008; Lenton, 2011) leading to possible positive feedbacks on the climate system (Leifeld et al., 2019; MacDougall et al., 2012). Increased land energy is related to decreases in soil moisture that may enhance the occurrence of extreme heat events (Jeong et al., 2016; Seneviratne et al., 2006, 2014, 2010; Xu et al., 2019). Such extreme events have demonstrated negative health effects in the most vulnerable sectors of the human and animal population (Matthews et al., 2017; McPherson et al., 2017; Sherwood and Huber, 2010; Watts et al., 2019). Given the importance of properly determining the fraction of EEI flowing into the land component, recent works have examined the CMIP5 simulations and revealed that Earth System Models (ESMs) have shortcomings in modelling the land heat content of the last half of the 20th century (Cuesta-Valero et al., 2016). Numerical experiments have pointed to an insufficient depth of the Land Surface Models (LSMs) (MacDougall et al., 2008, 2010; Stevens, 2007) and to a zero heat-flow bottom boundary condition (BBC) as the origin of the limitations in these simulations. A LSM of insufficient depth limits the amount of energy that can be stored in the subsurface. The zero heat-

https://doi.org/10.5194/essd-2019-255
Preprint. Discussion started: 20 March 2020
© Author(s) 2020. CC BY 4.0 License.


flow BBC neglects the small, but persistent long-term contribution from the flow of heat from the interior of the Earth, that shifts the thermal regime of the subsurface towards or away from the freezing point of water, such that the latent heat component is misrepresented (Hermoso de Mendoza et al., 2018). Although the heat from the interior of the Earth is constant at time scales of a few millennia, it may conflict with the setting of the LSM initial conditions in ESM simulations.

Borehole Climatology

The main premise of borehole climatology is that the subsurface thermal regime is determined by the balance of the heat flowing from the interior of the Earth (the bottom boundary condition) and the heat flowing through the interface between the lower atmosphere and the ground (the upper boundary condition). If the thermal properties of the subsurface are known, or if they can be assumed constant over short-depth intervals, then the thermal regime of the subsurface can be determined by the physics of heat diffusion. The simplest analogy is the temperature distribution along a (infinitely wide) cylinder with known thermal properties and constant temperature at both ends. If upper and lower boundary conditions remain constant (i.e. internal heat flow is constant, and there are no persistent variations on the ground surface energy balance), then the thermal regime of the subsurface is well known and it is in a (quasi) steady state. However, any change to the ground surface energy balance would create a transient, and such a change in the upper boundary condition would propagate into the ground leading to changes in the thermal regime of the subsurface (Beltrami, 2002). These changes in the ground surface energy balance propagate into the subsurface and are recorded as departures from the quasi-steady thermal state of the subsurface. Borehole climatology uses these subsurface temperature anomalies to reconstruct the ground surface temperature changes that may have been responsible for creating the subsurface temperature anomalies we observe. That is, it is an attempt to reconstruct the temporal evolution of the upper boundary condition. Ground Surface Temperature Histories (GSTHs) and Ground Heat Flux Histories (GHFHs) have been reconstructed from borehole temperature profile (BTP) measurements at regional and larger scales for decadal and millennial time-scales. (Barkaoui et al., 2013; Beck, 1977; Beltrami, 2001; Beltrami et al., 2006; Beltrami and Bourlon, 2004; Cermak, 1971; Chouinard and Mareschal, 2009; Davis et al., 2010; Demezhko and Gornostaeva, 2015; Harris and Chapman, 2001; Hartmann and Rath, 2005; Hopcroft et al., 2007; Huang et al., 2000; Jaume-Santero et al., 2016; Lachenbruch and Marshall, 1986; LANE, 1923; Pickler et al., 2018;

https://doi.org/10.5194/essd-2019-255
Preprint. Discussion started: 20 March 2020
© Author(s) 2020. CC BY 4.0 License.


551 Roy et al., 2002; Vasseur et al., 1983). These reconstructions have provided independent records
552 for the evaluation of the evolution of the climate system well before the existence of
553 meteorological records. Because subsurface temperatures are a direct measure, which unlike proxy
554 reconstructions of past climate do not need to be calibrated with the meteorological records, they
555 provide an independent way of assessing changes in climate. Such records, are useful tools for
556 evaluating climate simulations beyond the observational period (Beltrami et al., 2017; Cuesta-
557 Valero et al., 2016, 2019; García-García et al., 2016; González-Rouco et al., 2006, 2009; Jaume-
558 Santero et al., 2016; MacDougall et al., 2010; Stevens et al., 2008), as well as for assessing proxy
559 data reconstructions (Beltrami et al., 2017; Jaume-Santero etl., 2016).

560 **Land Heat Content Estimates**

561 Global continental energy content has been previously estimated from geothermal data retrieved
562 from a set of quality-controlled borehole temperature profiles. Ground heat content was estimated
563 from heat flux histories derived from BTP data (Beltrami, 2002a; Beltrami et al., 2002, 2006).
564 Such results have formed part of the estimate used in AR3, AR4 and AR5 IPCC reports (see Box
565 3.1, Chapter 3 (Rhein et al., 2013). A continental heat content estimate was inferred from
566 meteorological observations of surface air temperature since the beginning of the 20th century
567 (Huang, 2006). Nevertheless, all global estimates were performed nearly two decades ago. Since,
568 those days, advances in borehole methodological techniques (e.g., Beltrami et al., 2015; Cuesta-
569 Valero et al., 2016; Jaume-Santero et al., 2016), the availability of additional BTP measurements,
570 and the possibility of assessing the continental heat fluxes in the context of the FluxNet
571 measurements (Gentine et al., 2019) requires a comprehensive summary of all global ground heat
572 fluxes and continental heat content estimates.

573

Reference	Time period	Heat Flux (mWm^{-2})	Heat Content (ZJ)	Source of Data
Beltrami (2002a)	1950-2000	33	7.1	Geothermal
Beltrami (2002)	1950-2000	39.1 (3.5)	9.1 (0.8)	Geothermal

https://doi.org/10.5194/essd-2019-255
Preprint. Discussion started: 20 March 2020
© Author(s) 2020. CC BY 4.0 License.

Beltrami (2002)	1900-2000	34.1 (3.4)	15.9 (1.6)	Geothermal
Beltrami (2002)	1765-2000	20.0 (2.0)	25.7 (2.6)	Geothermal
Huang (2006)	1950-2000	-	6.7	Meteorological
Gentine et al (2020)	2004-2015	240 (120)	-	FluxNet, Geothermal, LSM
Cuesta-Valero et al (2020)	1950-2000	70 (20)	16 (3)	Geothermal
Cuesta-Valero et al (2020)	1950-2000	60 (30)	14 (6)	Geothermal
Cuesta-Valero et al (2020)	1950-2000	60 (20)	13 (5)	Geothermal
Cuesta-Valero et al (2020)	1993-2018	129 (28)	14 (3)	Geothermal
(Cuesta-Valero et al., (2020)	2004-2015	136 (28)	6 (1)	Geothermal

574 **Table 2.** Ground surface heat flux and global continental heat content. Uncertainties in parenthesis.

575

576

https://doi.org/10.5194/essd-2019-255
Preprint. Discussion started: 20 March 2020
© Author(s) 2020. CC BY 4.0 License.

Open Access Earth System Science Data Discussions

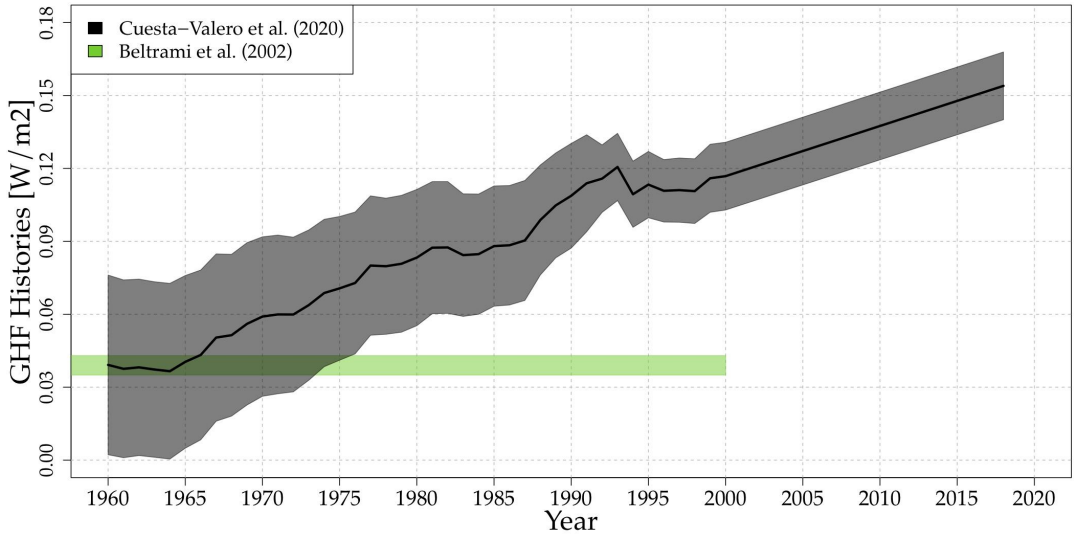

577
578
579 ***Figure 4:*** *Global mean ground heat flux history (black line) and 95% confidence interval (gray shadow)*
580 *from BTP measurements from Cuesta-Valero et al. (2020). Results for 1950-2000 from Beltrami et al.*
581 *(2002) (green bar) are provided for comparison purposes.*
582

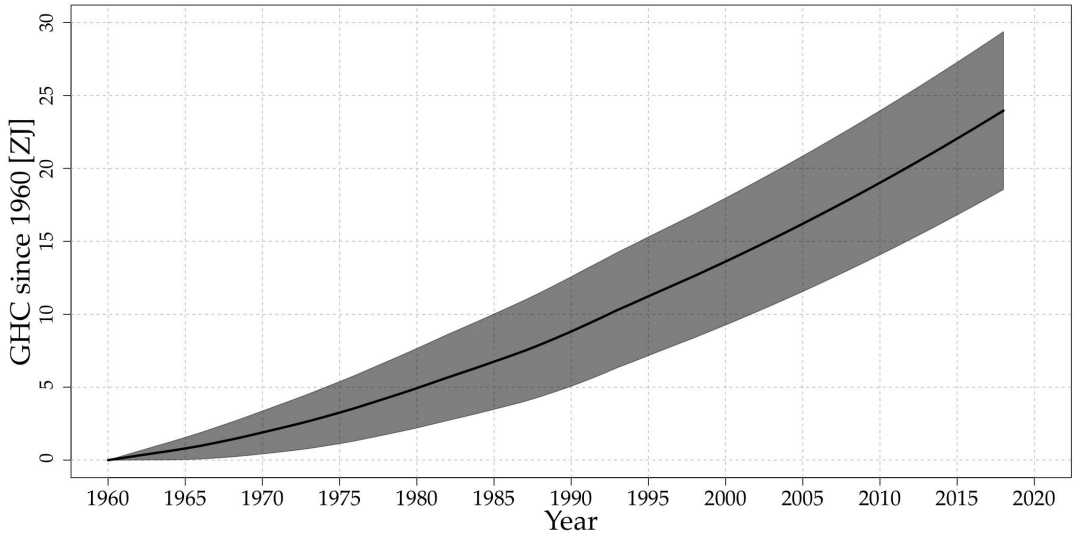

583
584 ***Figure 5:*** *Global cumulative heat storage within continental landmasses since 1960 CE (black line) and*
585 *95% confidence interval (gray shadow) from GHF results displayed in Fig.4. Data obtained from Cuesta-*
586 *Valero et al. (2020).*

https://doi.org/10.5194/essd-2019-255
Preprint. Discussion started: 20 March 2020
© Author(s) 2020. CC BY 4.0 License.


587 The first estimates of continental heat content used borehole temperature versus depth profile data.
588 However, the dataset in those analyses included borehole temperature profiles of a wide range of
589 depths, as well as different data acquisition dates. That is, each borehole profile contained the
590 record of the accumulation of heat in the subsurface for different time intervals. In addition the
591 borehole data were analyzed with a single model and a single constant value for each subsurface
592 thermal property.

593 Although the thermal signals are attenuated with depth, which may partially compensate data
594 shortcomings, uncertainties were introduced in the analysis and may have affected the estimates.
595 A continental heat content estimate was carried out using gridded meteorological product of
596 surface air temperature by (Huang, 2006). Such work yielded similar values as the estimates from
597 geothermal data (see Table 2). This estimate, however, assumed that surface air and ground
598 temperatures are perfectly coupled, and used a single value for the thermal conductivity of the
599 ground. Studies have shown that the coupling of the surface air and ground temperatures is
600 mediated by several processes that may influence the ground surface energy balance, and therefore,
601 the air-ground temperature coupling (García-García et al., 2019; Melo-Aguilar et al., 2018;
602 Stieglitz and Smerdon, 2007). In a novel attempt to reconcile continental heat content from soil
603 heat-plate data from the FluxNet network with estimates from geothermal data and a deep bottom-
604 boundary land surface model simulation, (Gentine et al., 2019) obtained a much larger magnitude
605 from the global land heat flux than all previous estimates. Cuesta-Valero et al. (2020) has recently
606 updated the estimate of the global continental heat content using a larger borehole temperature
607 database that includes more recent measurements and a stricter data quality control. This work
608 takes into account the differences in borehole logging time as well as restricts the data to the same
609 depth range for each borehole temperature profile, ensuring that the subsurface accumulation of
610 heat is synchronous. In addition to the standard method for reconstructing heat fluxes with a single
611 constant value for each subsurface thermal property, Cuesta-Valero et al. (2020) also developed a
612 new approach that considers a range of possible subsurface thermal properties, several models,
613 each at a range of resolutions yielding a more realistic range of uncertainties for the fraction of the
614 EEI flowing into the land subsurface.

615

616

https://doi.org/10.5194/essd-2019-255
Preprint. Discussion started: 20 March 2020
© Author(s) 2020. CC BY 4.0 License.


617 **Conclusion**

618 Global land heat content estimates from FluxNet data, geothermal data and model simulations
619 point to a marked increase in the amount of energy flowing into the ground in the last few decades
620 (Fig. 4, 5 and Table 2). These results are consistent with the observations of ocean, cryosphere and
621 atmospheric heat storage increases during the same time period and with EEI at the top of the
622 atmosphere.

623

624 ## 4. Heat utilized to melt ice

625

626 The energy uptake by the cryosphere is given by the sum of the energy uptake within each one of
627 its components: sea-ice, Greenland and Antarctic ice sheets, glaciers other than those that are part
628 of the ice sheets ('glaciers', hereafter), snow and permafrost. Within any component, in turn,
629 changes in energy are a result of phase changes (through the latent heat supplied to melt ice or that
630 released by freezing) and/or to any warming or cooling not associated with a phase change. An
631 explicit derivation of the energy change associated with changes in the different cryosphere
632 components and an estimate of the energy uptake for each component between 1960 and 2017 is
633 given in (Straneo et al., 2019a). Here we summarize the method, the data and model outputs used
634 for the estimates, but we refer to this study for more in depth details.

635

636 The cryosphere changes between 1960 and 2017 are dominated by changes occurring in the two
637 polar ice sheets, Arctic sea-ice and glaciers worldwide. Contributions from snow and permafrost
638 are neglected because they are small and/or associated with large uncertainties. We also neglect
639 any contribution from Antarctic sea-ice for which no clear trend in sea-ice extent has been
640 observed over the period of interest (Parkinson, 2019). In addition, for the components considered,
641 we neglect changes in the temperature of the remaining ice since the energy change associated
642 with these is negligible compared to the energy associated with the ice loss. As a result, the energy
643 change within each component is equal to the energy needed to melt the ice (i.e. warm it to the
644 freezing temperature and then supply the latent heat needed to melt the ice). For simplicity, and
645 consistent with previous estimates (Ciais et al., 2013), we use a constant latent heat of fusion of
646 3.34×10^5 J/kg, a specific heat capacity of 4000 J/kg C and a constant density of ice of 920 kg/m^3.

647

648 For Antarctica, we separate contributions from grounded ice loss and floating ice loss building on
649 recent separate estimates for each. Grounded ice loss from 1992 to 2017 is based on a recent study
650 that reconciles mass balance estimates from gravimetry, altimetry and input-output methods from
651 1992 to 2017 (Shepherd et al., 2018b) . From 1972 to 1991, we use the estimates from Rignot et
652 al. (2019) which combined modeled surface mass balance with ice discharge estimates from the
653 input/output method. Ice shelf thinning rates 1994 to 2017, based on new satellite altimetry

https://doi.org/10.5194/essd-2019-255
Preprint. Discussion started: 20 March 2020
© Author(s) 2020. CC BY 4.0 License.


reconstructions (Adusumilli et al., 2019; Straneo et al., 2019a), provide an estimate of the floating ice loss. In particular, these show that the floating ice loss from Antarctica since the 1990s exceeds the grounded ice loss. For Greenland, we combine mass balance estimates from a number of recent studies (Mankoff et al., 2019; Shepherd et al., 2018a), with estimates of tidewater glacier retreat, floating ice loss and firn layer temperature changes. For glaciers we combine estimates from the Randolph Glacier Inventory, for glaciers outside of Greenland and Antarctica, based on direct and geodetic measurements (Zemp et al., 2019), with estimates based on a glacier model forced with an ensemble of reanalysis data (Marzeion et al., 2015) and GRACE based estimates (Bamber et al., 2018). An additional contribution from uncharted glaciers or glaciers that have already disappeared is obtained from Parkes and Marzeion (2018) Greenland and Antarctic peripheral glaciers are derived from Zemp et al., (2019) and Marzeion et al. (2015). Finally, while estimates of Arctic sea-ice extent exist over the satellite record, sea-ice thickness distribution measurements are scarce making it challenging to estimate volume changes. Instead we use the Pan-Arctic Ice Ocean Modeling and Assimilation System (PIOMAS)(Schweiger et al., 2011; Zhang and Rothrock, 2003) which is validated with all available thickness and concentration data (from submarines, oceanographic moorings, and satellites; see Kwok (2018) and against multi-decadal records constructed from satellite (e.g. Laxon et al. 2013) and in-situ observations (Schweiger et al., 2011). A longer reconstruction using a slightly different model version, PIOMAS-20C (Schweiger et al., 2019), is used to cover the 1960 to 1978 period that is not covered by PIOMAS.

These reconstructions reveal that all four components contributed similar amounts (between 2-5 ZJ) over the 1960-2017 period amounting to a total energy uptake of 14.2 +/- 1.6 ZJ over this period (Straneo et al., 2019a). Compared to earlier estimates, and in particular the 8.83 ZJ estimate from (Ciais et al., 2013), this larger estimate is a result both of the longer period of time considered and, also, the improved estimates of ice loss across all components and, especially, the ice shelves in Antarctica. Approximately half of this energy uptake is associated with the melting of grounded ice, while the remaining half is associated with the melting of floating ice (ice shelves in Antarctica and Greenland, Arctic sea-ice).

5. The Earth heat inventory: Where does the energy go?

The Earth has been in radiative imbalance, with less energy exiting the top of the atmosphere than entering, since at least about 1970 and the Earth has gained substantial energy over the past 40 decades (Hansen, 2005; Rhein et al., 2013)(Hansen, 2005; Rhein et al., 2013). Due to the characteristics of the Earth system components, the ocean with its large mass and high heat capacity dominates the Earth heat inventory (Cheng et al., 2016, 2017; Rhein et al., 2013; von Schuckmann et al., 2016). The rest goes into grounded and floating ice melt, and warming the land and atmosphere.

https://doi.org/10.5194/essd-2019-255
Preprint. Discussion started: 20 March 2020
© Author(s) 2020. CC BY 4.0 License.

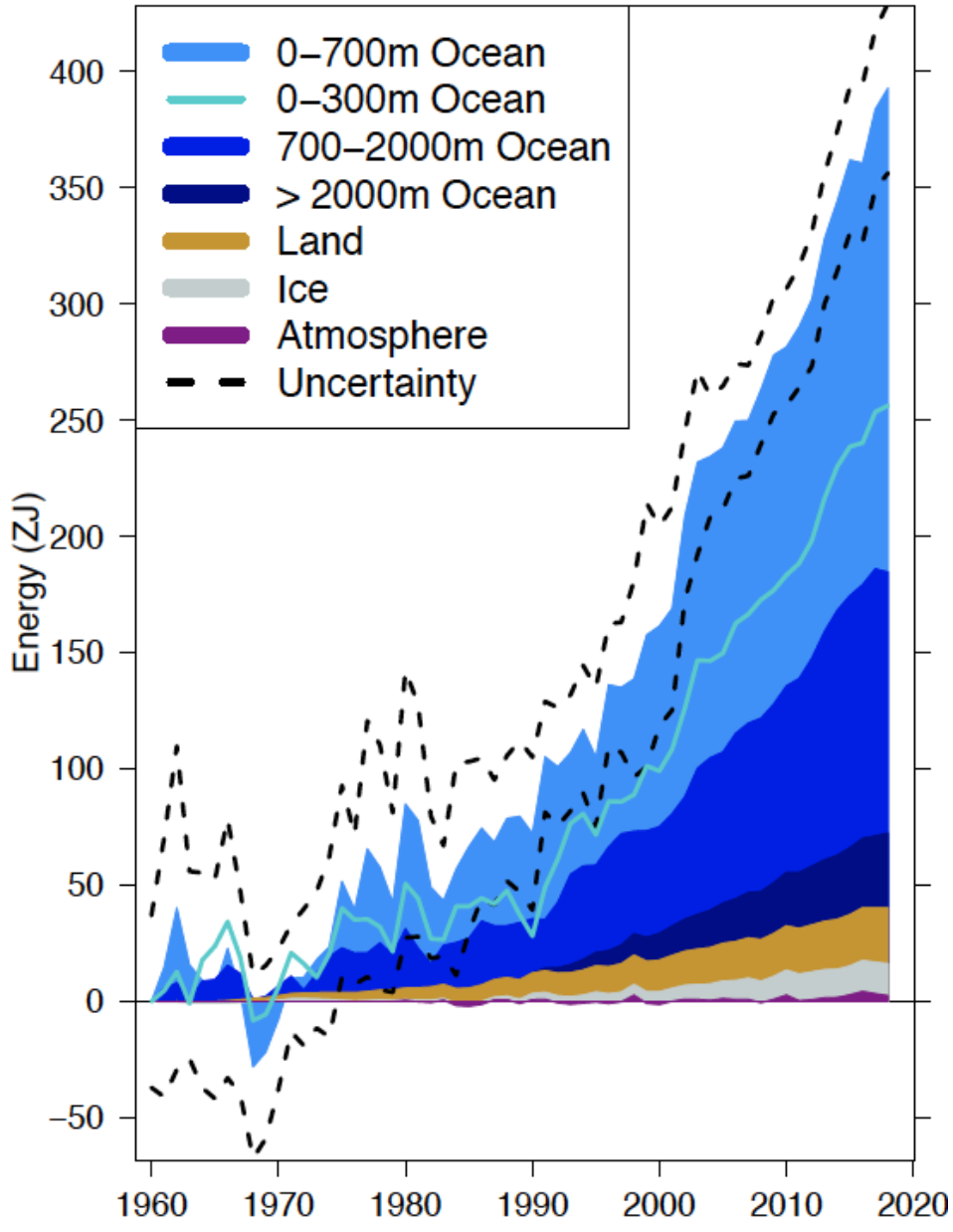

Figure 6: *Earth heat inventory (energy accumulation) in ZJ (1 ZJ = 10^{21} J) for the components of the Earth's climate system relative to 1960 and from 1960 to 2018 (assuming constant cryosphere increase for the years 2017 and 2018). See section 1-4 for data sources. The upper ocean (0-300m, light blue line, and*

https://doi.org/10.5194/essd-2019-255
Preprint. Discussion started: 20 March 2020
© Author(s) 2020. CC BY 4.0 License.

0-700m, light blue shading) account for the largest amount of heat gain, together with the intermediate ocean (700-2000m, blue shading), and the deep ocean below 2000m depth (dark blue shading). Although much lower, the second largest contributor is the storage of heat on land (orange shading), then followed by the gain of heat to melt grounded and floating ice in the cryosphere (gray shading). Due to its low heat capacity, the atmosphere (magenta shading) makes a smaller contribution. Uncertainty in the ocean estimate also dominates the total uncertainty (dot-dashed lines derived from the standard deviations (2-sigma) for the ocean, cryosphere and land. Atmospheric uncertainty is comparable small). The dataset for the Earth heat inventory is published at DKRZ (https://www.dkrz.de/) under the doi: https://doi.org/10.26050/WDCC/GCOS_EHI_EXP.

In agreement with previous studies, the Earth heat inventory based on most recent estimates of heat gain in the ocean (section 1), the atmosphere (section 2), land (section 3) and the cryosphere (section 4) shows a consistent long-term heat gain since the 1960s (Fig. 6). Our results show a total heat gain of 398 ± 40 ZJ over the period 1960-2018, which is equivalent to a heating rate of 0.42 ± 0.04 Wm^{-2} applied continuously over the surface area of the Earth (5.10 × 1014 m^2) over the past 58 years (assuming constant trend for cryosphere change for the years 2017 and 2018). The corresponding value for the period 1960-2016 amounts to 361 ± 40 ZJ and 0.40 ± 0.04 Wm^{-2}. The major player in the Earth inventory is the ocean, particularly the upper (0-700m) and intermediate (700-2000m) ocean layers (see also section 1, Fig. 2). Over the total period length 1960-2018, these two ocean layers accounted for 53% and 28% (Fig. 6). The deep ocean layer adds another 8%, so that the full-depth ocean contributes with 89% to the Earth heat inventory over the past 6 decades. Atmospheric warming amounts to 1% in the Earth heat inventory, the land heat gain with 6% and the heat gain in the cryosphere with 4%. These results show general agreement with previous estimates (e.g. Rhein et al., 2013), except for the ocean and land components: there is an increased amount of heat gain estimated for land, and a correspondingly lower heat storage change in the ocean estimated over the period 1960-2018.

We further analyse whether there is a change in where heat is stored in the Earth system over time. In particular, several papers have discussed a decline in the magnitude of EEI and the ocean heat gain during the 2000s, potentially linked to internal changes such as variations in Earth surface temperature rise or periods of strong climate variability (Dewitte et al., 2019; Smith et al., 2015). In agreement to the results obtained in section 1, there is an increased sequestration of heat into the deeper layers of the ocean. Compared to the periods 1960-2018 and 2000-2018, the Earth heat inventory for the upper ocean (0-700m) component is reduced by 5%, and 4% more heat is gained in the intermediate layers, and 2% in the deep ocean layer (Fig. 7). Moreover, there is an increase in heat gain in the atmosphere by 1%, i.e. a doubling of the atmospheric heat gain. Whether this observed regime shift in the Earth heat inventory is due to short-term (interannual to decadal scale) variations, or a consequence of unprecedented changes in the Earth system components from climate change needs further future evaluations.

https://doi.org/10.5194/essd-2019-255
Preprint. Discussion started: 20 March 2020
© Author(s) 2020. CC BY 4.0 License.

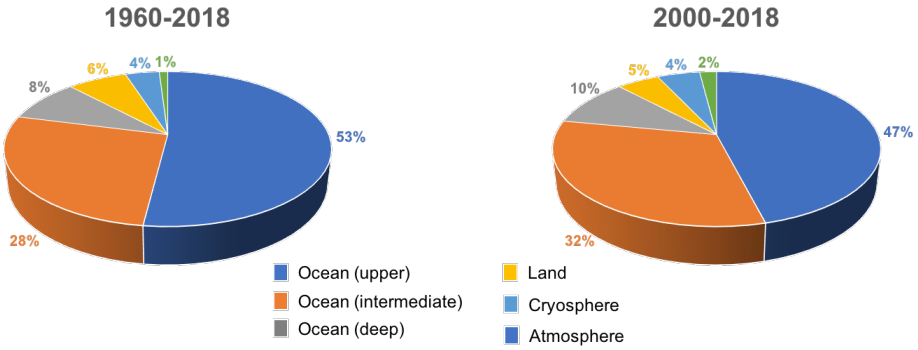

Figure 7: *Partition (in %) of the Earth heat inventory for the different components: ocean (upper: 0-700m, intermediate: 700-2000m, deep: > 2000m), land, cryosphere (grounded and floating ice) and atmosphere, for two different periods 1960-2018 and 2000-2018. Rates of change in ZJ/year over the period from the time series in Fig. 6 have been used to obtain the partitions.*

Immediate priorities include the maintenance and extension of the global climate observing system to assure a continuous monitoring of the Earth heat inventory, and to reduce the uncertainties. For the global ocean observing system, the core Argo sampling needs to be sustained, and complemented by remote sensing data. Extensions such as into the deep ocean layer need to be further fostered, and technical developments for the measurements under ice and in shallower areas need to be sustained. For the land component, a global monitoring program is urgently needed for the systematic measurement of land temperatures and ensuring a continuity of continental heat-gain estimates. Such an initiative should focus on areas with poor borehole temperature data coverage such as Africa, South America and the Arctic regions. In addition, repeating measurements at the same sites should be done whenever possible, as data taken after a decade or more at the same location would help to reduce uncertainties in the estimates.

For the atmosphere, the continuation of operational satellite- and ground-based observations is important but foremost sustaining and enhancing a coherent long-term monitoring system for the provision of climate data records of essential climate variables. GNSS radio occultation (RO) observations and reference radiosonde stations within the Global Climate Observing System (GCOS) Reference Upper Air Network (GRUAN) are regarded as climate benchmark observations. Operational RO missions for continuous global climate observations need to be maintained and expanded, ensuring global coverage over all local times, as backbone of a global climate observing system. Finally, sustained remote sensing for all of the cryosphere components is key to quantifying future changes. For sea-ice, both area and thickness are essential, as well as albedo. For ice sheets and glaciers, reliable measurements of ice thickness and extent, gravity, snow/firn thickness and density are essential to quantify changes in mass balance of grounded and floating ice. In all cases, remote sensing measurements have to be calibrated and validated by in situ measurements.

https://doi.org/10.5194/essd-2019-255
Preprint. Discussion started: 20 March 2020
© Author(s) 2020. CC BY 4.0 License.

Open Access Earth System Science Data Discussions

A continuous effort to regularly update the Earth heat inventory is important to quantify how much and where heat is stored in the climate system accumulated from climate change. The estimate of the Earth heat inventory is a multi-disciplinary task, and can only be achieved through concerted international effort. A regular quantification of the Earth heat inventory will not only deliver insight on the status of global climate change, but also provide a fundamental tool for the improvement and validation of climate projections. Moreover, the quantification of the Earth heat inventory needs to evolve in the future to include further estimates such as for example from ocean reanalyses, indirect estimates from remote sensing, as well as the inclusion of measurements of the EEI at the Top of the Atmosphere.

Data availability: The time series of the Earth heat inventory are published at DKRZ (https://www.dkrz.de/) under the doi: https://doi.org/10.26050/WDCC/GCOS_EHI_EXP (von Schuckmann et al., 2020). The data contain an updated international assessment of ocean warming estimates, and new and updated estimates of heat gain in the atmosphere, cryosphere and land over the period 1960-2018. This published dataset has been used to build the basis for Figure 6 and 7 of this manuscript. The ocean warming estimate is based on an international assessment of 15 different in situ data-based ocean products as presented in section 1. The new estimate of the atmospheric heat content is fully described in section 2, and is backboned on a combined use of atmospheric reanalyses, multi-satellite data records, and microwave sounding techniques. The land heat storage time series as presented in section 3 relies on borehole data. The heat available to account for cryosphere loss is presented in section 4, and is based on a combined use of model results and observations to obtain estimates of major cryosphere components such as polar ice sheets, Arctic sea-ice and glaciers.

GCOS Earth heat inventory team: Author contributions

Coordination: Karina von Schuckmann[1], Lijing Cheng[2], Matthew D. Palmer[3], Caterina Tassone[4], Valentin Aich[4]

Ocean: Karina von Schuckmann[1], Lijing Cheng[2], Tim Boyer[7], Damien Desbruyères[8], Catia Domingues[9,10], John Gilson[12], Masayoshi Ishii[15], Gregory C. Johnson[16], Rachel Killick[3], Brian A. King[9], Nicolas Kolodziejczyk[17], John Lyman[15], Maeva Monier[19], Didier Paolo Monselesan[20], Sarah Purkey[5], Dean Roemmich[5], Susan E. Wijffels[20,25]

Atmosphere: Andrea K. Steiner[13], Gottfried Kirchengast[13], Maximilian Gorfer[13], Michael Mayer[14], Leopold Haimberger[14]

https://doi.org/10.5194/essd-2019-255
Preprint. Discussion started: 20 March 2020
© Author(s) 2020. CC BY 4.0 License.

Land: Almudena García-García[6], Francisco José Cuesta-Valero[6], Hugo Beltrami[6], Sonia I. Seneviratne[22], Pierre Gentine[11]

Cryosphere: Fiammetta Straneo[5], Susheel Adusumilli[5], Donald A. Slater[5], Mary-Louise Timmermans[24], Ben Marzeion[18], Axel Schweiger[21], Andrew Shepherd[23]

Earth energy inventory: all authors, with specific contributions from Almudena García-García[6] and Francisco José Cuesta-Valero[6]

[1]Mercator Ocean International, France
[2]Institute of Atmospheric Physics, Chinese Academy of Sciences, China
[3]Met Office Hadley Centre, UK
[4]WMO/GCOS, Switzerland
[5]Scripps Institution of Oceanography, UCSD, USA
[6]Climate and Atmospheric Sciences Institute, and Environmental Sciences Program, St. Francis Xavier University, Canada
[7]NOAA's National Centers for Environmental Information
[8]University of Brest, CNRS, IRD, Ifremer, IUEM, France.
[9]National Oceanographic Centre, UK
[10]ARC Centre of Excellence for Climate Extremes, University of Tasmania, Hobart, Tasmania, Australia
[11]Earth and Environmental Engineering in the School of Engineering and Applied Sciences, Columbia University, USA
[12]University of California, USA
[13]Wegener Center for Climate and Global Change, University of Graz, Austria
[14]Institute of Meteorology and Geophysics, University of Vienna, Austria
[15]Department of Atmosphere, Ocean and Earth System Modeling Research, Meteorological Research Institute, Japan
[16]NOAA, Pacific Marine Environmental Laboratory, USA
[17] Ifremer, University of Brest, CNRS, IRD, Laboratoire d'Océanographie Physique et Spatiale, IUEM, France
[18]Institute of Geography, University of Bremen, Bremen, Germany
[19]CELAD/Mercator Ocean International, France
[20]CSIRO Oceans and Atmosphere, Hobart, Tasmania, Australia
[21]Applied Physics Laboratory, University of Washington, Seattle, USA
[22]Institute for Atmospheric and Climate Science, ETH, Switzerland
[23]Center for Polar Observation and Modeling, University of Leeds, Leeds, UK
[24]Department of Geology and Geophysics, Yale University, New Haven, USA
[25]Woods Hole Oceanographic Institution, Massachusetts, United States

Acknowledgements:

Ocean: PMEL contribution number 5053; Funding: CMD was supported by an ARC Future Fellowship (FT130101532).

Atmosphere: The authors express their gratitude to SPARC for supporting this activity under sponsorship of the WCRP. We acknowledge the WEGC EOPAC team for providing the OPSv5.6 RO data (available online at https://doi.org/10.25364/WEGC/OPS5.6:2019.1) as well as quality-

https://doi.org/10.5194/essd-2019-255
Preprint. Discussion started: 20 March 2020
© Author(s) 2020. CC BY 4.0 License.

processed Vaisala RS data, UCAR/CDAAC (Boulder, CO, USA) for access to RO phase and orbit data, RSS (Santa Rosa, CA, USA) for providing MSU V4.0 data, ECMWF (Reading, UK) for access to operational analysis and forecast data, ERA5 reanalysis data, and RS data from the ERA-Interim archive, JMA (Tokyo, Japan) for provision of the JRA-55 and JRA-55C reanalysis data, and NASA GMAO (Greenbelt, MD, USA) for access of the MERRA-2 reanalysis data.

Land: This work was supported by grants from the National Sciences and Engineering Research Council of Canada Discovery Grant (NSERC DG 140576948) and the Canada Research Chairs Program (CRC 230687) to H. Beltrami. Almudena García-García and Francisco José Cuesta-Valero are funded by Beltrami's CRC program, the School of Graduate Studies at Memorial University of Newfoundland and the Research Office at St. Francis Xavier University

References:

Abraham, J. P., Baringer, M., Bindoff, N. L., Boyer, T., Cheng, L. J., Church, J. A., Conroy, J. L., Domingues, C. M., Fasullo, J. T., Gilson, J., Goni, G., Good, S. A., Gorman, J. M., Gouretski, V., Ishii, M., Johnson, G. C., Kizu, S., Lyman, J. M., Macdonald, A. M., Minkowycz, W. J., Moffitt, S. E., Palmer, M. D., Piola, A. R., Reseghetti, F., Schuckmann, K., Trenberth, K. E., Velicogna, I. and Willis, J. K.: A review of global ocean temperature observations: Implications for ocean heat content estimates and climate change, Rev. Geophys., 51(3), 450–483, doi:10.1002/rog.20022, 2013.

Adusumilli, S., Fricker, H. A., Medley, B., Padman, L. and Siegfried, M. R.: Multi-year variability in ocean-driven melting of Antarctica's ice shelves, Nat. Geosci., under review, 2019.

Angerer, B., Ladstädter, F., Scherllin-Pirscher, B., Schwärz, M., Steiner, A. K., Foelsche, U. and Kirchengast, G.: Quality aspects of the Wegener Center multi-satellite GPS radio occultation record OPSv5.6, Atmos. Meas. Tech., 10(12), 4845–4863, doi:10.5194/amt-10-4845-2017, 2017.

Baggenstos, D., Häberli, M., Schmitt, J., Shackleton, S. A., Birner, B., Severinghaus, J. P., Kellerhals, T. and Fischer, H.: Earth's radiative imbalance from the Last Glacial Maximum to the present, Proc. Natl. Acad. Sci., 116(30), 14881, doi:10.1073/pnas.1905447116, 2019.

Bailey, V. L., Pries, C. H. and Lajtha, K.: What do we know about soil carbon destabilization?, Environ. Res. Lett., 14(8), 083004, doi:10.1088/1748-9326/ab2c11, 2019.

Bamber, J. L., Westaway, R. M., Marzeion, B. and Wouters, B.: The land ice contribution to sea level during the satellite era, Environ. Res. Lett., 13(6), 063008, doi:10.1088/1748-9326/aac2f0, 2018.

https://doi.org/10.5194/essd-2019-255
Preprint. Discussion started: 20 March 2020
© Author(s) 2020. CC BY 4.0 License.

Barkaoui, A. E., Correia, A., Zarhloule, Y., Rimi, A., Carneiro, J., Boughriba, M. and Verdoya, M.: Reconstruction of remote climate change from borehole temperature measurement in the eastern part of Morocco, Clim. Change, 118(2), 431–441, doi:10.1007/s10584-012-0638-7, 2013.

Beck, A. E.: Climatically perturbed temperature gradients and their effect on regional and continental heat-flow means, Tectonophysics, 41(1), 17–39, doi:https://doi.org/10.1016/0040-1951(77)90178-0, 1977.

Beltrami, H.: Surface heat flux histories from inversion of geothermal data: Energy balance at the Earth's surface, J. Geophys. Res. Solid Earth, 106(B10), 21979–21993, doi:10.1029/2000JB000065, 2001.

Beltrami, H.: Earth's Long-Term Memory, Science (80-.)., 297(5579), 206, doi:10.1126/science.1074027, 2002.

Beltrami, H. and Bourlon, E.: Ground warming patterns in the Northern Hemisphere during the last five centuries, Earth Planet. Sci. Lett., 227(3), 169–177, doi:https://doi.org/10.1016/j.epsl.2004.09.014, 2004.

Beltrami, H., Bourlon, E., Kellman, L. and González-Rouco, J. F.: Spatial patterns of ground heat gain in the Northern Hemisphere, Geophys. Res. Lett., 33(6), doi:10.1029/2006GL025676, 2006.

Beltrami, H., Matharoo, G. S. and Smerdon, J. E.: Impact of borehole depths on reconstructed estimates of ground surface temperature histories and energy storage, J. Geophys. Res. Earth Surf., 120(5), 763–778, doi:10.1002/2014JF003382, 2015.

Beltrami, H., Matharoo, G. S., Smerdon, J. E., Illanes, L. and Tarasov, L.: Impacts of the Last Glacial Cycle on ground surface temperature reconstructions over the last millennium, Geophys. Res. Lett., 44(1), 355–364, doi:10.1002/2016GL071317, 2017.

Berrisford, P., Kållberg, P., Kobayashi, S., Dee, D., Uppala, S., Simmons, A. J., Poli, P. and Sato, H.: Atmospheric conservation properties in ERA-Interim, Q. J. R. Meteorol. Soc., 137(659), 1381–1399, doi:10.1002/qj.864, 2011.

Bopp, L., Resplandy, L., Orr, J. C., Doney, S. C., Dunne, J. P., Gehlen, M., Halloran, P., Heinze, C., Ilyina, T., Séférian, R., Tjiputra, J. and Vichi, M.: Multiple stressors of ocean ecosystems in the 21st century: projections with CMIP5 models, Biogeosciences, 10(10), 6225–6245, doi:10.5194/bg-10-6225-2013, 2013.

Boyer, T., Domingues, C. M., Good, S. A., Johnson, G. C., Lyman, J. M., Ishii, M., Gouretski, V., Willis, J. K., Antonov, J., Wijffels, S., Church, J. A., Cowley, R. and Bindoff, N. L.: Sensitivity of Global Upper-Ocean Heat Content Estimates to Mapping Methods, XBT Bias Corrections, and Baseline Climatologies, J. Clim., 29(13), 4817–4842, doi:10.1175/JCLI-D-15-0801.1, 2016.

Breitburg, D., Levin, L. A., Oschlies, A., Grégoire, M., Chavez, F. P., Conley, D. J., Garçon, V.,

https://doi.org/10.5194/essd-2019-255
Preprint. Discussion started: 20 March 2020
© Author(s) 2020. CC BY 4.0 License.

938 Gilbert, D., Gutiérrez, D., Isensee, K., Jacinto, G. S., Limburg, K. E., Montes, I., Naqvi, S. W.
939 A., Pitcher, G. C., Rabalais, N. N., Roman, M. R., Rose, K. A., Seibel, B. A., Telszewski, M.,
940 Yasuhara, M. and Zhang, J.: Declining oxygen in the global ocean and coastal waters, Science
941 (80-.)., 359(6371), eaam7240, doi:10.1126/science.aam7240, 2018.

942 Cabanes, C., Grouazel, A., Von Schuckmann, K., Hamon, M., Turpin, V., Coatanoan, C., Paris,
943 F., Guinehut, S., Boone, C., Ferry, N., De Boyer Montégut, C., Carval, T., Reverdin, G.,
944 Pouliquen, S. and Le Traon, P. Y.: The CORA dataset: Validation and diagnostics of in-situ
945 ocean temperature and salinity measurements, Ocean Sci., 9(1), 1–18, doi:10.5194/os-9-1-2013,
946 2013.

947 Capotondi, A., Alexander, M. A., Bond, N. A., Curchitser, E. N. and Scott, J. D.: Enhanced
948 upper ocean stratification with climate change in the CMIP3 models, J. Geophys. Res. Ocean.,
949 117(C4), doi:10.1029/2011JC007409, 2012.

950 Cermak, V.: Underground temperature and inferred climatic temperature of the past millenium,
951 Palaeogeogr. Palaeoclimatol. Palaeoecol., 10(1), 1–19, doi:10.1016/0031-0182(71)90043-5,
952 1971.

953 Cheng, L., Trenberth, K. E., Palmer, M. D., Zhu, J. and Abraham, J. P.: Observed and simulated
954 full-depth ocean heat-content changes for 1970–2005, Ocean Sci., 12(4), 925–935,
955 doi:10.5194/os-12-925-2016, 2016.

956 Cheng, L., Trenberth, K. E., Fasullo, J., Boyer, T., Abraham, J. and Zhu, J.: Improved estimates
957 of ocean heat content from 1960 to 2015, Sci. Adv., 3(3), e1601545,
958 doi:10.1126/sciadv.1601545, 2017.

959 Cheng, L., Abraham, J., Hausfather, Z. and Trenberth, K. E.: How fast are the oceans warming?,
960 Science (80-.)., 363(6423), 128, doi:10.1126/science.aav7619, 2019.

961 Chiodo, G. and Haimberger, L.: Interannual changes in mass consistent energy budgets from
962 ERA-Interim and satellite data, J. Geophys. Res. Atmos., 115(D2), doi:10.1029/2009JD012049,
963 2010.

964 Chouinard, C. and Mareschal, J.-C.: Ground surface temperature history in southern Canada:
965 Temperatures at the base of the Laurentide ice sheet and during the Holocene, Earth Planet. Sci.
966 Lett., 277(1–2), 280–289, doi:10.1016/j.epsl.2008.10.026, 2009.

967 Ciais, P., Sabine, C., Bala, G., Bopp, L., Brovkin, V., Canadell, J., Chhabra, A., DeFries, R.,
968 Galloway, J., Heimann, M., Jones, C., Quéré, C. Le, Myneni, R. B., Piao, S. and Thornton, P.:
969 The physical science basis. Contribution of working group I to the fifth assessment report of the
970 intergovernmental panel on climate change, Chang. IPCC Clim., 465–570,
971 doi:10.1017/CBO9781107415324.015, 2013.

972 Clark, P. U., Shakun, J. D., Marcott, S. A., Mix, A. C., Eby, M., Kulp, S., Levermann, A., Milne,
973 G. A., Pfister, P. L., Santer, B. D., Schrag, D. P., Solomon, S., Stocker, T. F., Strauss, B. H.,
974 Weaver, A. J., Winkelmann, R., Archer, D., Bard, E., Goldner, A., Lambeck, K., Pierrehumbert,
975 R. T. and Plattner, G.-K.: Consequences of twenty-first-century policy for multi-millennial

https://doi.org/10.5194/essd-2019-255
Preprint. Discussion started: 20 March 2020
© Author(s) 2020. CC BY 4.0 License.

976 climate and sea-level change, Nat. Clim. Chang., 6(4), 360–369, doi:10.1038/nclimate2923,
977 2016.

978 Cohen, J., Screen, J. A., Furtado, J. C., Barlow, M., Whittleston, D., Coumou, D., Francis, J.,
979 Dethloff, K., Entekhabi, D., Overland, J. and Jones, J.: Recent Arctic amplification and extreme
980 mid-latitude weather, Nat. Geosci., 7(9), 627–637, doi:10.1038/ngeo2234, 2014.

981 Coumou, D., Di Capua, G., Vavrus, S., Wang, L. and Wang, S.: The influence of Arctic
982 amplification on mid-latitude summer circulation, Nat. Commun., 9(1), 2959,
983 doi:10.1038/s41467-018-05256-8, 2018.

984 Cuesta-Valero, F., Garcia-Garcia, A., Beltrami, H., Gonzalez-Rouco, F. and Garcia-Bustamante,
985 E.: Long-Term Global Changes in Ground Surface Temperature and Ground Surface Heat Flux
986 from Geothermal Data, J. Geophys. Res.- Earth Surf., submitted, 2020.

987 Cuesta-Valero, F. J., García-García, A., Beltrami, H. and Smerdon, J. E.: First assessment of
988 continental energy storage in CMIP5 simulations, Geophys. Res. Lett., 43(10), 5326–5335,
989 doi:10.1002/2016GL068496, 2016.

990 Cuesta-Valero, F. J., García-García, A., Beltrami, H., Zorita, E. and Jaume-Santero, F.: Long-
991 term Surface Temperature (LoST) database as a complement for GCM preindustrial simulations,
992 Clim. Past, 15(3), 1099–1111, doi:10.5194/cp-15-1099-2019, 2019.

993 Davis, M. G., Harris, R. N. and Chapman, D. S.: Repeat temperature measurements in boreholes
994 from northwestern Utah link ground and air temperature changes at the decadal time scale, J.
995 Geophys. Res. Solid Earth, 115(B5), doi:10.1029/2009JB006875, 2010.

996 Demezhko, D. Y. and Gornostaeva, A. A.: Late Pleistocene–Holocene ground surface heat flux
997 changes reconstructed from borehole temperature data (the Urals, Russia), Clim. Past, 11(4),
998 647–652, doi:10.5194/cp-11-647-2015, 2015.

999 Desbruyères, D. G., Purkey, S. G., McDonagh, E. L., Johnson, G. C. and King, B. A.: Deep and
1000 abyssal ocean warming from 35 years of repeat hydrography, Geophys. Res. Lett., 43(19), 10,
1001 310–356, 365, doi:10.1002/2016GL070413, 2016.

1002 Dewitte, S., Clerbaux, N. and Cornelis, J.: Decadal Changes of the Reflected Solar Radiation and
1003 the Earth Energy Imbalance, Remote Sens., 11(6), 663, doi:10.3390/rs11060663, 2019.

1004 Dieng, H. B., Cazenave, A., Meyssignac, B. and Ablain, M.: New estimate of the current rate of
1005 sea level rise from a sea level budget approach, Geophys. Res. Lett., 44(8), 3744–3751,
1006 doi:10.1002/2017GL073308, 2017.

1007 Fischer, E. M. and Knutti, R.: Observed heavy precipitation increase confirms theory and early
1008 models, Nat. Clim. Chang., 6(11), 986–991, doi:10.1038/nclimate3110, 2016.

1009 Frölicher, T. L., Fischer, E. M. and Gruber, N.: Marine heatwaves under global warming, Nature,
1010 560(7718), 360–364, doi:10.1038/s41586-018-0383-9, 2018.

https://doi.org/10.5194/essd-2019-255
Preprint. Discussion started: 20 March 2020
© Author(s) 2020. CC BY 4.0 License.

1011 Fu, Q., Solomon, S., Pahlavan, H. A. and Lin, P.: Observed changes in Brewer–Dobson
1012 circulation for 1980–2018, Environ. Res. Lett., 14(11), 114026, doi:10.1088/1748-9326/ab4de7,
1013 2019.

1014 García Molinos, J., Halpern, B. S., Schoeman, D. S., Brown, C. J., Kiessling, W., Moore, P. J.,
1015 Pandolfi, J. M., Poloczanska, E. S., Richardson, A. J. and Burrows, M. T.: Climate velocity and
1016 the future global redistribution of marine biodiversity, Nat. Clim. Chang., 6(1), 83–88,
1017 doi:10.1038/nclimate2769, 2016.

1018 García-García, A., Cuesta-Valero, F. J., Beltrami, H. and Smerdon, J. E.: Simulation of air and
1019 ground temperatures in PMIP3/CMIP5 last millennium simulations: implications for climate
1020 reconstructions from borehole temperature profiles, Environ. Res. Lett., 11(4), 044022,
1021 doi:10.1088/1748-9326/11/4/044022, 2016.

1022 García-García, A., Cuesta-Valero, F. J., Beltrami, H. and Smerdon, J. E.: Characterization of Air
1023 and Ground Temperature Relationships within the CMIP5 Historical and Future Climate
1024 Simulations, J. Geophys. Res. Atmos., 124(7), 3903–3929, doi:10.1029/2018JD030117, 2019.

1025 Gardner, A. S., Moholdt, G., Cogley, J. G., Wouters, B., Arendt, A. A., Wahr, J., Berthier, E.,
1026 Hock, R., Pfeffer, W. T., Kaser, G., Ligtenberg, S. R. M., Bolch, T., Sharp, M. J., Hagen, J. O.,
1027 van den Broeke, M. R. and Paul, F.: A Reconciled Estimate of Glacier Contributions to Sea
1028 Level Rise: 2003 to 2009, Science (80-.)., 340(6134), 852, doi:10.1126/science.1234532, 2013.

1029 Gattuso, J.-P., Magnan, A., Billé, R., Cheung, W. W. L., Howes, E. L., Joos, F., Allemand, D.,
1030 Bopp, L., Cooley, S. R., Eakin, C. M., Hoegh-Guldberg, O., Kelly, R. P., Pörtner, H.-O., Rogers,
1031 A. D., Baxter, J. M., Laffoley, D., Osborn, D., Rankovic, A., Rochette, J., Sumaila, U. R.,
1032 Treyer, S. and Turley, C.: Contrasting futures for ocean and society from different anthropogenic
1033 CO₂ emissions scenarios, Science (80-.)., 349(6243), aac4722,
1034 doi:10.1126/science.aac4722, 2015.

1035 Gelaro, R., McCarty, W., Suárez, M. J., Todling, R., Molod, A., Takacs, L., Randles, C. A.,
1036 Darmenov, A., Bosilovich, M. G., Reichle, R., Wargan, K., Coy, L., Cullather, R., Draper, C.,
1037 Akella, S., Buchard, V., Conaty, A., da Silva, A. M., Gu, W., Kim, G.-K., Koster, R., Lucchesi,
1038 R., Merkova, D., Nielsen, J. E., Partyka, G., Pawson, S., Putman, W., Rienecker, M., Schubert,
1039 S. D., Sienkiewicz, M. and Zhao, B.: The Modern-Era Retrospective Analysis for Research and
1040 Applications, Version 2 (MERRA-2), J. Clim., 30(14), 5419–5454, doi:10.1175/JCLI-D-16-
1041 0758.1, 2017.

1042 Gentine, P., Garcia-Garcia, A., Meier, R., Cuesta-Valero, F., Hugo., B., Davin, E. L. and
1043 Seneviratne, S. I.: Large recent continental heat storage, Nature, under revi, 2019.

1044 Gleckler, P., Durack, P., Ronald, S., Johnson, G. and Forest, C.: Industrial-era global ocean heat
1045 uptake doubles in recent decades, Nat. Clim. Chang., 6, doi:10.1038/nclimate2915, 2016.

1046 Goni, G. J., Sprintall, J., Bringas, F., Cheng, L., Cirano, M., Dong, S., Domingues, R., Goes, M.,
1047 Lopez, H., Morrow, R., Rivero, U., Rossby, T., Todd, R. E., Trinanes, J., Zilberman, N.,
1048 Baringer, M., Boyer, T., Cowley, R., Domingues, C. M., Hutchinson, K., Kramp, M., Mata, M.
1049 M., Reseghetti, F., Sun, C., Bhaskar TVS, U. and Volkov, D.: More Than 50 Years of Successful

https://doi.org/10.5194/essd-2019-255
Preprint. Discussion started: 20 March 2020
© Author(s) 2020. CC BY 4.0 License.

1050 Continuous Temperature Section Measurements by the Global Expendable Bathythermograph
1051 Network, Its Integrability, Societal Benefits, and Future, Front. Mar. Sci., 6, 452 [online]
1052 Available from: https://www.frontiersin.org/article/10.3389/fmars.2019.00452, 2019.

1053 González-Rouco, J. F., Beltrami, H., Zorita, E. and von Storch, H.: Simulation and inversion of
1054 borehole temperature profiles in surrogate climates: Spatial distribution and surface coupling,
1055 Geophys. Res. Lett., 33(1), doi:10.1029/2005GL024693, 2006.

1056 González-Rouco, J. F., Beltrami, H., Zorita, E. and Stevens, M. B.: Borehole climatology: a
1057 discussion based on contributions from climate modeling, Clim. Past, 5(1), 97–127,
1058 doi:10.5194/cp-5-97-2009, 2009.

1059 Good, S. A., Martin, M. J. and Rayner, N. A.: EN4: Quality controlled ocean temperature and
1060 salinity profiles and monthly objective analyses with uncertainty estimates, J. Geophys. Res.
1061 Ocean., 118(12), 6704–6716, doi:10.1002/2013JC009067, 2013.

1062 Gregory, J. M. and Andrews, T.: Variation in climate sensitivity and feedback parameters during
1063 the historical period, Geophys. Res. Lett., 43(8), 3911–3920, doi:10.1002/2016GL068406, 2016.

1064 Guinehut, S., Dhomps, A.-L., Larnicol, G. and Le Traon, P.-Y.: High resolution 3-D temperature
1065 and salinity fields derived from in situ and satellite observations, Ocean Sci., 8(5), 845–857,
1066 doi:10.5194/os-8-845-2012, 2012.

1067 Hansen, J.: Efficacy of climate forcings, J. Geophys. Res., 110(D18), D18104,
1068 doi:10.1029/2005JD005776, 2005.

1069 Hansen, J., Sato, M., Kharecha, P. and von Schuckmann, K.: Earth's energy imbalance and
1070 implications, Atmos. Chem. Phys., 11(24), 13421–13449, doi:10.5194/acp-11-13421-2011,
1071 2011.

1072 Harris, R. N. and Chapman, D. S.: Mid-latitude (30°–60° N) climatic warming inferred by
1073 combining borehole temperatures with surface air temperatures, Geophys. Res. Lett., 28(5), 747–
1074 750, doi:10.1029/2000GL012348, 2001.

1075 Hartmann, A. and Rath, V.: Uncertainties and shortcomings of ground surface temperature
1076 histories derived from inversion of temperature logs, J. Geophys. Eng., 2(4), 299–311,
1077 doi:10.1088/1742-2132/2/4/S02, 2005.

1078 Hermoso de Mendoza, I., Beltrami, H., MacDougall, A. H. and Mareschal, J.-C.: Lower
1079 boundary conditions in Land Surface Models. Effects on the permafrost and the carbon pools,
1080 Geosci. Model Dev. Discuss., 2018, 1–34, doi:10.5194/gmd-2018-233, 2018.

1081 Hersbach, H., Rosnay, P. de, Bell, B., Schepers, D., Simmons, A., Soci, C., Abdalla, S., Alonso-
1082 Balmaseda, M., Balsamo, G., Bechtold, P., Berrisford, P., Bidlot, J.-R., de Boisséson, E.,
1083 Bonavita, M., Browne, P., Buizza, R., Dahlgren, P., Dee, D., Dragani, R., Diamantakis, M.,
1084 Flemming, J., Forbes, R., Geer, A. J., Haiden, T., Hólm, E., Haimberger, L., Hogan, R., Horányi,
1085 A., Janiskova, M., Laloyaux, P., Lopez, P., Munoz-Sabater, J., Peubey, C., Radu, R., Richardson,
1086 D., Thépaut, J.-N., Vitart, F., Yang, X., Zsótér, E. and Zuo, H.: Operational global reanalysis:

https://doi.org/10.5194/essd-2019-255
Preprint. Discussion started: 20 March 2020
© Author(s) 2020. CC BY 4.0 License.

progress, future directions and synergies with NWP. [online] Available from: https://www.ecmwf.int/node/18765, 2018.

Hersbach, H., Bell, W., Berrisford, P., Horányi, A., Muñoz-Sabater, J., Nicolas, J., Radu, R., Schepers, D., Simmons, A., Soci, C. and Dee, D.: Global reanalysis: goodbye ERA-Interim, hello ERA5, ECMWF Newsl., (159) [online] Available from: https://www.ecmwf.int/node/19027, 2019.

Hicks Pries, C. E., Castanha, C., Porras, R. and Torn, M. S.: The whole-soil carbon flux in response to warming, Science (80-.)., eaal1319, doi:10.1126/science.aal1319, 2017.

Hoegh-Guldberg, O., et al.: Global Warming on Natural and Human Systems. In: Global Warming of 1.5°C. An IPCC Special Report on the impacts of global warming of 1.5°C above pre-industrial levels and related global greenhouse gas emission pathways, in the context of strengthening the global response to the threat of climate change, sustainable development, and efforts to eradicate poverty., 2018.

Hopcroft, P. O., Gallagher, K. and Pain, C. C.: Inference of past climate from borehole temperature data using Bayesian Reversible Jump Markov chain Monte Carlo, Geophys. J. Int., 171(3), 1430–1439, doi:10.1111/j.1365-246X.2007.03596.x, 2007.

Huang, S.: 1851–2004 annual heat budget of the continental landmasses, Geophys. Res. Lett., 33(4), doi:10.1029/2005GL025300, 2006.

Huang, S., Pollack, H. N. and Shen, P.-Y.: Temperature trends over the past five centuries reconstructed from borehole temperatures, Nature, 403(6771), 756–758, doi:10.1038/35001556, 2000.

Irving, D. B., Wijffels, S. and Church, J. A.: Anthropogenic Aerosols, Greenhouse Gases, and the Uptake, Transport, and Storage of Excess Heat in the Climate System, Geophys. Res. Lett., 46(9), 4894–4903, doi:10.1029/2019GL082015, 2019.

Ishii, M., Fukuda, Y., Hirahara, S., Yasui, S., Suzuki, T. and Sato, K.: Accuracy of Global Upper Ocean Heat Content Estimation Expected from Present Observational Data Sets, SOLA, 13, 163–167, doi:10.2151/sola.2017-030, 2017.

Jacobs, S. S., Giulivi, C. F. and Mele, P. A.: Freshening of the Ross Sea During the Late 20th Century, Science (80-.)., 297(5580), 386, doi:10.1126/science.1069574, 2002.

Jaume-Santero, F., Pickler, C., Beltrami, H. and Mareschal, J.-C.: North American regional climate reconstruction from ground surface temperature histories, Clim. Past, 12(12), 2181–2194, doi:10.5194/cp-12-2181-2016, 2016.

Jeong, D. Il, Sushama, L., Diro, G. T., Khaliq, M. N., Beltrami, H. and Caya, D.: Projected changes to high temperature events for Canada based on a regional climate model ensemble, Clim. Dyn., 46(9), 3163–3180, doi:10.1007/s00382-015-2759-y, 2016.

Johnson, G.C., Lyman, J.M. , Boyer, T., Cheng, L., Domingues, C.M., Gilson, J., Ishii, M.,

https://doi.org/10.5194/essd-2019-255
Preprint. Discussion started: 20 March 2020
© Author(s) 2020. CC BY 4.0 License.

1123 Killick, R., Monselesan, D., Purkey, S.G., Wijffels, S. E.: Ocean heat content [in State of the
1124 Climate in 2017], Bull. Am. Meteorol. Soc., 99(8), S72–S77, 2018.

1125 Johnson, G. C., Purkey, S. G., Zilberman, N. V and Roemmich, D.: Deep Argo Quantifies
1126 Bottom Water Warming Rates in the Southwest Pacific Basin, Geophys. Res. Lett., 46(5), 2662–
1127 2669, doi:10.1029/2018GL081685, 2019.

1128 King, B. A., Firing, E. and M.Joyce, T.: Chapter 3.1 Shipboard observations during WOCE, Int.
1129 Geophys., 77, 99–122, doi:10.1016/S0074-6142(01)80114-5, 2001.

1130 Kirchengast, G., Ladstädter, F., Steiner, A. K., Gorfer, M., Lippl, F. and Angerer, B.: Climate
1131 trends and variability in atmosphere heat content and atmosphere-ocean heat exchanges: space
1132 geodesy is key. [online] Available from: https://www.czech-
1133 in.org/cmPortalV15/CM_W3_Searchable/iugg19/normal#!sessiondetails/0000119801_0, 2019.

1134 Knutti, R. and Rugenstein, M. A. A.: Feedbacks, climate sensitivity and the limits of linear
1135 models, Philos. Trans. R. Soc. A Math. Phys. Eng. Sci., 373(2054), 20150146,
1136 doi:10.1098/rsta.2015.0146, 2015.

1137 Kobayashi, S., Ota, Y., Harada, Y., Ebita, A., Moriya, M., Onoda, H., Onogi, K., Kamahori, H.,
1138 Kobayashi, C., Endo, H., MiyaokaI, K. and Takahashi, K.: The JRA-55 Reanalysis: General
1139 Specifications and Basic Characteristics, J. Meteorol. Soc. Japan. Ser. II, 93(1), 5–48,
1140 doi:10.2151/jmsj.2015-001, 2015.

1141 Kuhlbrodt, T. and Gregory, J. M.: Ocean heat uptake and its consequences for the magnitude of
1142 sea level rise and climate change, Geophys. Res. Lett., 39(18), doi:10.1029/2012GL052952,
1143 2012.

1144 Kwok, R.: Arctic sea ice thickness, volume, and multiyear ice coverage: losses and coupled
1145 variability (1958–2018), Environ. Res. Lett., 13(10), 105005, doi:10.1088/1748-9326/aae3ec,
1146 2018.

1147 Lachenbruch, A. H. and Marshall, B. V.: Changing Climate: Geothermal Evidence from
1148 Permafrost in the Alaskan Arctic, Science (80-.)., 234(4777), 689–696 [online] Available from:
1149 www.jstor.org/stable/1697932, 1986.

1150 LANE, A. C.: Geotherms of Lake Superior Copper Country, GSA Bull., 34(4), 703–720,
1151 doi:10.1130/GSAB-34-703, 1923.

1152 Leifeld, J., Wüst-Galley, C. and Page, S.: Intact and managed peatland soils as a source and sink
1153 of GHGs from 1850 to 2100, Nat. Clim. Chang., 9(12), 945–947, doi:10.1038/s41558-019-0615-
1154 5, 2019.

1155 Lembo, V., Folini, D., Wild, M. and Lionello, P.: Inter-hemispheric differences in energy
1156 budgets and cross-equatorial transport anomalies during the 20th century, Clim. Dyn., 53(1),
1157 115–135, doi:10.1007/s00382-018-4572-x, 2019.

1158 Lenton, T., Rockström, J., Gaffney, O., Rahmstorf, S., Richardson, K., Steffen, W. and

https://doi.org/10.5194/essd-2019-255
Preprint. Discussion started: 20 March 2020
© Author(s) 2020. CC BY 4.0 License.

1159 Schellnhuber, H.: Climate tipping points — too risky to bet against, Nature, 575, 592–595,
1160 doi:10.1038/d41586-019-03595-0, 2019.

1161 Lenton, T. M.: Early warning of climate tipping points, Nat. Clim. Chang., 1(4), 201–209,
1162 doi:10.1038/nclimate1143, 2011.

1163 Lenton, T. M., Held, H., Kriegler, E., Hall, J. W., Lucht, W., Rahmstorf, S. and Schellnhuber, H.
1164 J.: Tipping elements in the Earth's climate system., Proc. Natl. Acad. Sci. U. S. A., 105(6),
1165 1786–93, doi:10.1073/pnas.0705414105, 2008.

1166 Levitus, S., Antonov, J. I., Boyer, T. P., Baranova, O. K., Garcia, H. E., Locarnini, R. A.,
1167 Mishonov, A. V, Reagan, J. R., Seidov, D., Yarosh, E. S. and Zweng, M. M.: World ocean heat
1168 content and thermosteric sea level change (0–2000 m), 1955–2010, Geophys. Res. Lett., 39(10),
1169 doi:10.1029/2012GL051106, 2012.

1170 Llovel, W., Willis, J. K., Landerer, F. W. and Fukumori, I.: Deep-ocean contribution to sea level
1171 and energy budget not detectable over the past decade, Nat. Clim. Chang., 4(11), 1031–1035,
1172 doi:10.1038/nclimate2387, 2014.

1173 Loeb, N. G., Lyman, J. M., Johnson, G. C., Allan, R. P., Doelling, D. R., Wong, T., Soden, B. J.
1174 and Stephens, G. L.: Observed changes in top-of-the-atmosphere radiation and upper-ocean
1175 heating consistent within uncertainty, Nat. Geosci., 5(2), 110–113, doi:10.1038/ngeo1375, 2012.

1176 Loeb, N. G., Wang, H., Cheng, A., Kato, S., Fasullo, J. T., Xu, K.-M. and Allan, R. P.:
1177 Observational constraints on atmospheric and oceanic cross-equatorial heat transports: revisiting
1178 the precipitation asymmetry problem in climate models, Clim. Dyn., 46(9), 3239–3257,
1179 doi:10.1007/s00382-015-2766-z, 2016.

1180 MacDougall, A. H., González-Rouco, J. F., Stevens, M. B. and Beltrami, H.: Quantification of
1181 subsurface heat storage in a GCM simulation, Geophys. Res. Lett., 35(13),
1182 doi:10.1029/2008GL034639, 2008.

1183 MacDougall, A. H., Beltrami, H., González-Rouco, J. F., Stevens, M. B. and Bourlon, E.:
1184 Comparison of observed and general circulation model derived continental subsurface heat flux
1185 in the Northern Hemisphere, J. Geophys. Res. Atmos., 115(D12), doi:10.1029/2009JD013170,
1186 2010.

1187 MacDougall, A. H., Avis, C. A. and Weaver, A. J.: Significant contribution to climate warming
1188 from the permafrost carbon feedback, Nat. Geosci., 5(10), 719–721, doi:10.1038/ngeo1573,
1189 2012.

1190 Mankoff, K. D., Colgan, W., Solgaard, A., Karlsson, N. B., Ahlstrøm, A. P., van As, D., Box, J.
1191 E., Khan, S. A., Kjeldsen, K. K., Mouginot, J. and Fausto, R. S.: Greenland Ice Sheet solid ice
1192 discharge from 1986 through 2017, Earth Syst. Sci. Data, 11(2), 769–786, doi:10.5194/essd-11-
1193 769-2019, 2019.

1194 Marshall, J., Scott, J. R., Armour, K. C., Campin, J.-M., Kelley, M. and Romanou, A.: The
1195 ocean's role in the transient response of climate to abrupt greenhouse gas forcing, Clim. Dyn.,

https://doi.org/10.5194/essd-2019-255
Preprint. Discussion started: 20 March 2020
© Author(s) 2020. CC BY 4.0 License.

1196 44(7), 2287–2299, doi:10.1007/s00382-014-2308-0, 2015.

1197 Marzeion, B., Leclercq, P. W., Cogley, J. G. and Jarosch, A. H.: Brief Communication: Global
1198 reconstructions of glacier mass change during the 20th century are consistent, Cryosph., 9(6),
1199 2399–2404, doi:10.5194/tc-9-2399-2015, 2015.

1200 Masson-Delmotte, V., Schulz, M., Abe-Ouchi, A., Beer, J., Ganopolski, A., Rouco, J. F. G.,
1201 Jansen, E., Lambeck, K., Luterbacher, J., Naish, T., Osborn, T., Otto-Bliesner, B., Quinn, T.,
1202 Ramesh, R., Rojas, M., Shao, X. and Timmermann, A.: Information from Paleoclimate Archives.
1203 In: Climate Change 2013: The Physical Science Basis. Contribution of Working Group I to the
1204 Fifth Assessment Report of the Intergovernmental Panel on Climate Change [Stocker, T.F., D.
1205 Qin, G.-K. Plattner, M. Tignor, Cambridge University Press, Cambridge, United Kingdom and
1206 New York, NY, USA., 2013.

1207 Matthews, T. K. R., Wilby, R. L. and Murphy, C.: Communicating the deadly consequences of
1208 global warming for human heat stress, Proc. Natl. Acad. Sci., 114(15), 3861,
1209 doi:10.1073/pnas.1617526114, 2017.

1210 Mayer, M., Haimberger, L., Edwards, J. M. and Hyder, P.: Toward Consistent Diagnostics of the
1211 Coupled Atmosphere and Ocean Energy Budgets, J. Clim., 30(22), 9225–9246,
1212 doi:10.1175/JCLI-D-17-0137.1, 2017.

1213 Mayer, M., Tietsche, S., Haimberger, L., Tsubouchi, T., Mayer, J. and Zuo, H.: An Improved
1214 Estimate of the Coupled Arctic Energy Budget, J. Clim., 32(22), 7915–7934, doi:10.1175/JCLI-
1215 D-19-0233.1, 2019.

1216 McPherson, M., García-García, A., Cuesta-Valero Francisco, J., Beltrami, H., Hansen-Ketchum,
1217 P., MacDougall, D. and Ogden Nicholas, H.: Expansion of the Lyme Disease Vector Ixodes
1218 Scapularis in Canada Inferred from CMIP5 Climate Projections, Environ. Health Perspect.,
1219 125(5), 057008, doi:10.1289/EHP57, 2017.

1220 Mears, C. A. and Wentz, F. J.: Construction of the Remote Sensing Systems V3.2 Atmospheric
1221 Temperature Records from the MSU and AMSU Microwave Sounders, J. Atmos. Ocean.
1222 Technol., 26(6), 1040–1056, doi:10.1175/2008JTECHA1176.1, 2009a.

1223 Mears, C. A. and Wentz, F. J.: Construction of the RSS V3.2 Lower-Tropospheric Temperature
1224 Dataset from the MSU and AMSU Microwave Sounders, J. Atmos. Ocean. Technol., 26(8),
1225 1493–1509, doi:10.1175/2009JTECHA1237.1, 2009b.

1226 Mears, C. A. and Wentz, F. J.: A Satellite-Derived Lower-Tropospheric Atmospheric
1227 Temperature Dataset Using an Optimized Adjustment for Diurnal Effects, J. Clim., 30(19),
1228 7695–7718, doi:10.1175/JCLI-D-16-0768.1, 2017.

1229 Melo-Aguilar, C., González-Rouco, J. F., García-Bustamante, E., Navarro-Montesinos, J. and
1230 Steinert, N.: Influence of radiative forcing factors on ground–air temperature coupling during the
1231 last millennium: implications for borehole climatology, Clim. Past, 14(11), 1583–1606,
1232 doi:10.5194/cp-14-1583-2018, 2018.

https://doi.org/10.5194/essd-2019-255
Preprint. Discussion started: 20 March 2020
© Author(s) 2020. CC BY 4.0 License.

1233 Meyssignac, B., Boyer, T., Zhao, Z., Hakuba, M. Z., Landerer, F. W., Stammer, D., Köhl, A.,
1234 Kato, S., L'Ecuyer, T., Ablain, M., Abraham, J. P., Blazquez, A., Cazenave, A., Church, J. A.,
1235 Cowley, R., Cheng, L., Domingues, C. M., Giglio, D., Gouretski, V., Ishii, M., Johnson, G. C.,
1236 Killick, R. E., Legler, D., Llovel, W., Lyman, J., Palmer, M. D., Piotrowicz, S., Purkey, S. G.,
1237 Roemmich, D., Roca, R., Savita, A., Schuckmann, K. von, Speich, S., Stephens, G., Wang, G.,
1238 Wijffels, S. E. and Zilberman, N.: Measuring Global Ocean Heat Content to Estimate the Earth
1239 Energy Imbalance, Front. Mar. Sci., 6, 432 [online] Available from:
1240 https://www.frontiersin.org/article/10.3389/fmars.2019.00432, 2019.

1241 Myhre, G., Shindell, D., Bréon, F.-M., Collins, W., Fuglestvedt, J., Huang, J., Koch, D.,
1242 Lamarque, J.-F., Lee, D., Mendoza, B., Nakajima, T., Robock, A., Stephens, G., Takemura, T.
1243 and Zhang, H.: Anthropogenic and natural radiative forcing, in Climate Change 2013 the
1244 Physical Science Basis: Working Group I Contribution to the Fifth Assessment Report of the
1245 Intergovernmental Panel on Climate Change, vol. 9781107057, pp. 659–740, Cambridge
1246 University Press, Cambridge, United Kingdom and New York, NY, USA., 2013.

1247 Nauels, A., Meinshausen, M., Mengel, M., Lorbacher, K. and Wigley, T. M. L.: Synthesizing
1248 long-term sea level rise projections – the MAGICC sea level model v2.0, Geosci. Model Dev.,
1249 10(6), 2495–2524, doi:10.5194/gmd-10-2495-2017, 2017.

1250 Palmer, M. D., Roberts, C. D., Balmaseda, M., Chang, Y.-S., Chepurin, G., Ferry, N., Fujii, Y.,
1251 Good, S. A., Guinehut, S., Haines, K., Hernandez, F., Köhl, A., Lee, T., Martin, M. J., Masina,
1252 S., Masuda, S., Peterson, K. A., Storto, A., Toyoda, T., Valdivieso, M., Vernieres, G., Wang, O.
1253 and Xue, Y.: Ocean heat content variability and change in an ensemble of ocean reanalyses,
1254 Clim. Dyn., 49(3), 909–930, doi:10.1007/s00382-015-2801-0, 2017.

1255 Palmer, M. D., Harris, G. R. and Gregory, J. M.: Extending CMIP5 projections of global mean
1256 temperature change and sea level rise due to thermal expansion using a physically-based
1257 emulator, Environ. Res. Lett., 13(8), 084003, doi:10.1088/1748-9326/aad2e4, 2018.

1258 Parkes, D. and Marzeion, B.: Twentieth-century contribution to sea-level rise from uncharted
1259 glaciers, Nature, 563(7732), 551–554, doi:10.1038/s41586-018-0687-9, 2018.

1260 Parkinson, C. L.: A 40-y record reveals gradual Antarctic sea ice increases followed by decreases
1261 at rates far exceeding the rates seen in the Arctic, Proc. Natl. Acad. Sci., 116(29), 14414,
1262 doi:10.1073/pnas.1906556116, 2019.

1263 Peixoto, J. P. and Oort, A. H.: Physics of climate, New York, NY (United States); American
1264 Institute of Physics, United States. [online] Available from:
1265 https://www.osti.gov/servlets/purl/7287064, 1992.

1266 Pickler, C., Fausto, E., Beltrami, H., Mareschal, jean-claude, Suárez, F., Chacon-Oecklers, A.,
1267 Blin, N., Calderón, M., Montenegro, A., Harris, R. and Tassara, A.: Recent climate variations in
1268 Chile: Constraints from borehole temperature profiles, Clim. Past, 14, 559–575, doi:10.5194/cp-
1269 14-559-2018, 2018.

1270 Polyakov, I. V, Pnyushkov, A. V, Alkire, M. B., Ashik, I. M., Baumann, T. M., Carmack, E. C.,
1271 Goszczko, I., Guthrie, J., Ivanov, V. V, Kanzow, T., Krishfield, R., Kwok, R., Sundfjord, A.,

https://doi.org/10.5194/essd-2019-255
Preprint. Discussion started: 20 March 2020
© Author(s) 2020. CC BY 4.0 License.

1272 Morison, J., Rember, R. and Yulin, A.: Greater role for Atlantic inflows on sea-ice loss in the
1273 Eurasian Basin of the Arctic Ocean, Science (80-.)., 356(6335), 285,
1274 doi:10.1126/science.aai8204, 2017.

1275 Pritchard, H. D., Ligtenberg, S. R. M., Fricker, H. A., Vaughan, D. G., van den Broeke, M. R.
1276 and Padman, L.: Antarctic ice-sheet loss driven by basal melting of ice shelves, Nature,
1277 484(7395), 502–505, doi:10.1038/nature10968, 2012.

1278 Purkey, S. G. and Johnson, G. C.: Warming of Global Abyssal and Deep Southern Ocean Waters
1279 between the 1990s and 2000s: Contributions to Global Heat and Sea Level Rise Budgets, J.
1280 Clim., 23(23), 6336–6351, doi:10.1175/2010JCLI3682.1, 2010.

1281 Ramírez, F., Afán, I., Davis, L. S. and Chiaradia, A.: Climate impacts on global hot spots of
1282 marine biodiversity, Sci. Adv., 3(2), e1601198, doi:10.1126/sciadv.1601198, 2017.

1283 Rhein, M., Rintoul, S., Aoki, S., Campos, E., Chambers, D., Feely, R., Gulev, S., Johnson, G.,
1284 Josey, S., Kostianoy, A., Mauritzen, C., Roemmich, D., Talley, L. and Wang, F.: Observations:
1285 Ocean. In: Climate Change 2013: The Physical Science Basis. Contribution of Working Group I
1286 to the Fifth Assessment Report of the Intergovernmental Panel on Climate Change], Cambridge
1287 University Press, Cambridge United Kingdom and New York, USA., 2013.

1288 Rhein, M., Steinfeldt, R., Huhn, O., Sültenfuß, J. and Breckenfelder, T.: Greenland Submarine
1289 Melt Water Observed in the Labrador and Irminger Sea, Geophys. Res. Lett., 45(19), 10, 510–
1290 570, 578, doi:10.1029/2018GL079110, 2018.

1291 Rignot, E., Mouginot, J., Scheuchl, B., van den Broeke, M., van Wessem, M. J. and Morlighem,
1292 M.: Four decades of Antarctic Ice Sheet mass balance from 1979–2017, Proc. Natl. Acad. Sci.,
1293 116(4), 1095, doi:10.1073/pnas.1812883116, 2019.

1294 Riser, S. C., Freeland, H. J., Roemmich, D., Wijffels, S., Troisi, A., Belbéoch, M., Gilbert, D.,
1295 Xu, J., Pouliquen, S., Thresher, A., Le Traon, P.-Y., Maze, G., Klein, B., Ravichandran, M.,
1296 Grant, F., Poulain, P.-M., Suga, T., Lim, B., Sterl, A., Sutton, P., Mork, K.-A., Vélez-Belchí, P.
1297 J., Ansorge, I., King, B., Turton, J., Baringer, M. and Jayne, S. R.: Fifteen years of ocean
1298 observations with the global Argo array, Nat. Clim. Chang., 6(2), 145–153,
1299 doi:10.1038/nclimate2872, 2016.

1300 Roemmich, D. and Gilson, J.: The 2004–2008 mean and annual cycle of temperature, salinity,
1301 and steric height in the global ocean from the Argo Program, Prog. Oceanogr., 82(2), 81–100,
1302 doi:https://doi.org/10.1016/j.pocean.2009.03.004, 2009.

1303 Roy, S., Harris, R. N., Rao, R. U. M. and Chapman, D. S.: Climate change in India inferred from
1304 geothermal observations, J. Geophys. Res. Solid Earth, 107(B7), ETG 5-1-ETG 5-16,
1305 doi:10.1029/2001JB000536, 2002.

1306 Santer, B. D., Solomon, S., Wentz, F. J., Fu, Q., Po-Chedley, S., Mears, C., Painter, J. F. and
1307 Bonfils, C.: Tropospheric Warming Over The Past Two Decades, Sci. Rep., 7(1), 2336,
1308 doi:10.1038/s41598-017-02520-7, 2017.

https://doi.org/10.5194/essd-2019-255
Preprint. Discussion started: 20 March 2020
© Author(s) 2020. CC BY 4.0 License.

1309 Santer, B. D., Po-Chedley, S., Zelinka, M. D., Cvijanovic, I., Bonfils, C., Durack, P. J., Fu, Q.,
1310 Kiehl, J., Mears, C., Painter, J., Pallotta, G., Solomon, S., Wentz, F. J. and Zou, C.-Z.: Human
1311 influence on the seasonal cycle of tropospheric temperature, Science (80-.)., 361(6399),
1312 eaas8806, doi:10.1126/science.aas8806, 2018.

1313 von Schuckmann, K. and Le Traon, P.-Y.: How well can we derive Global Ocean Indicators
1314 from Argo data?, Ocean Sci., 7(6), 783–791, doi:10.5194/os-7-783-2011, 2011.

1315 von Schuckmann, K., Sallée, J.-B., Chambers, D., Le Traon, P.-Y., Cabanes, C., Gaillard, F.,
1316 Speich, S. and Hamon, M.: Consistency of the current global ocean observing systems from an
1317 Argo perspective, Ocean Sci., 10(3), 547–557, doi:10.5194/os-10-547-2014, 2014.

1318 von Schuckmann, K., Palmer, M. D., Trenberth, K. E., Cazenave, A., Chambers, D.,
1319 Champollion, N., Hansen, J., Josey, S. A., Loeb, N., Mathieu, P.-P., Meyssignac, B. and Wild,
1320 M.: An imperative to monitor Earth's energy imbalance, Nat. Clim. Chang., 6(2), 138–144,
1321 doi:10.1038/nclimate2876, 2016.

1322 von Schuckmann, K., Le Traon, P.-Y., Smith, N., Pascual, A., Brasseur, P., Fennel, K.,
1323 Djavidnia, S., Aaboe, S., Fanjul, E. A., Autret, E., Axell, L., Aznar, R., Benincasa, M., Bentamy,
1324 A., Boberg, F., Bourdallé-Badie, R., Nardelli, B. B., Brando, V. E., Bricaud, C., Breivik, L.-A.,
1325 Brewin, R. J. W., Capet, A., Ceschin, A., Ciliberti, S., Cossarini, G., de Alfonso, M., de Pascual
1326 Collar, A., de Kloe, J., Deshayes, J., Desportes, C., Drévillon, M., Drillet, Y., Droghei, R.,
1327 Dubois, C., Embury, O., Etienne, H., Fratianni, C., Lafuente, J. G., Sotillo, M. G., Garric, G.,
1328 Gasparin, F., Gerin, R., Good, S., Gourrion, J., Grégoire, M., Greiner, E., Guinehut, S.,
1329 Gutknecht, E., Hernandez, F., Hernandez, O., Høyer, J., Jackson, L., Jandt, S., Josey, S., Juza,
1330 M., Kennedy, J., Kokkini, Z., Korres, G., Kõuts, M., Lagemaa, P., Lavergne, T., le Cann, B.,
1331 Legeais, J.-F., Lemieux-Dudon, B., Levier, B., Lien, V., Maljutenko, I., Manzano, F., Marcos,
1332 M., Marinova, V., Masina, S., Mauri, E., Mayer, M., Melet, A., Mélin, F., Meyssignac, B.,
1333 Monier, M., Müller, M., Mulet, S., Naranjo, C., Notarstefano, G., Paulmier, A., Gomez, B. P.,
1334 Gonzalez, I. P., Peneva, E., Perruche, C., Andrew Peterson, K., Pinardi, N., Pisano, A., Pardo, S.,
1335 Poulain, P.-M., Raj, R. P., Raudsepp, U., Ravdas, M., Reid, R., Rio, M.-H., Salon, S.,
1336 Samuelsen, A., Sammartino, M., et al.: Copernicus Marine Service Ocean State Report, J. Oper.
1337 Oceanogr., 11(sup1), S1–S142, doi:10.1080/1755876X.2018.1489208, 2018.

1338

1339 von Schuckmann, K., Cheng, L., Palmer, M. D., Tassone, C., Aich, V., Adusumilli, S., Beltrami,
1340 H., Boyer, T., Cuesta-Valero, F. J., Desbruyeres, D., Domingues, C., García-García, A., Gentine,
1341 P., Gilson, J., Gorfer, M., Haimberger, L., Ishii, M., Johnson, G. C., Killick, R., King, B. A.,
1342 Kirchengast, G., Kolodziejczyk, N., Lyman, J., Marzeion, B., Mayer, M., Monier, M.,
1343 Monselesan, D. P., Purkey, S., Roemmich, D., Schweiger, A., Seneviratne, S. I., Shepherd, A.,
1344 Slater, D. A., Steiner, A. K., Straneo, F., Timmermanns, M.-L. and Wijffels, S. E.: Heat stored in
1345 the Earth system: Where does the energy go?, World Data Center for Climate (WDCC) at
1346 DKRZ, doi:10.26050/WDCC/GCOS_EHI_EXP, 2020.
1347

1348 Schweiger, A., Lindsay, R., Zhang, J., Steele, M., Stern, H. and Kwok, R.: Uncertainty in

https://doi.org/10.5194/essd-2019-255
Preprint. Discussion started: 20 March 2020
© Author(s) 2020. CC BY 4.0 License.

1349 modeled Arctic sea ice volume, J. Geophys. Res. Ocean., 116(C8), doi:10.1029/2011JC007084,
1350 2011.

1351 Schweiger, A. J., Wood, K. R. and Zhang, J.: Arctic Sea Ice Volume Variability over 1901–
1352 2010: A Model-Based Reconstruction, J. Clim., 32(15), 4731–4752, doi:10.1175/JCLI-D-19-
1353 0008.1, 2019.

1354 Seneviratne, S., Lüthi, D., Litschi, M. and Schär, C.: Land-atmosphere coupling and climate
1355 change in Europe, Nature, 443, 205–209, doi:10.1038/nature05095, 2006.

1356 Seneviratne, S., Donat, M., Mueller, B. and Alexander, L.: No pause in the increase of hot
1357 temperature extremes, Nat. Clim. Chang., 4, doi:10.1038/nclimate2145, 2014.

1358 Seneviratne, S. I., Corti, T., Davin, E. L., Hirschi, M., Jaeger, E. B., Lehner, I., Orlowsky, B. and
1359 Teuling, A. J.: Investigating soil moisture–climate interactions in a changing climate: A review,
1360 Earth-Science Rev., 99(3–4), 125–161, doi:10.1016/J.EARSCIREV.2010.02.004, 2010.

1361 Serreze, M. C. and Barry, R. G.: Processes and impacts of Arctic amplification: A research
1362 synthesis, Glob. Planet. Change, 77(1–2), 85–96, doi:10.1016/J.GLOPLACHA.2011.03.004,
1363 2011.

1364 Shepherd, A., Ivins, E., Rignot, E., Smith, B., van den Broeke, M., Velicogna, I., Whitehouse, P.,
1365 Briggs, K., Joughin, I., Krinner, G., Nowicki, S., Payne, T., Scambos, T., Schlegel, N., A, G.,
1366 Agosta, C., Ahlstrøm, A., Babonis, G., Barletta, V., Blazquez, A., Bonin, J., Csatho, B.,
1367 Cullather, R., Felikson, D., Fettweis, X., Forsberg, R., Gallee, H., Gardner, A., Gilbert, L., Groh,
1368 A., Gunter, B., Hanna, E., Harig, C., Helm, V., Horvath, A., Horwath, M., Khan, S., Kjeldsen, K.
1369 K., Konrad, H., Langen, P., Lecavalier, B., Loomis, B., Luthcke, S., McMillan, M., Melini, D.,
1370 Mernild, S., Mohajerani, Y., Moore, P., Mouginot, J., Moyano, G., Muir, A., Nagler, T., Nield,
1371 G., Nilsson, J., Noel, B., Otosaka, I., Pattle, M. E., Peltier, W. R., Pie, N., Rietbroek, R., Rott, H.,
1372 Sandberg-Sørensen, L., Sasgen, I., Save, H., Scheuchl, B., Schrama, E., Schröder, L., Seo, K.-
1373 W., Simonsen, S., Slater, T., Spada, G., Sutterley, T., Talpe, M., Tarasov, L., van de Berg, W. J.,
1374 van der Wal, W., van Wessem, M., Vishwakarma, B. D., Wiese, D., Wouters, B. and team, T. I.:
1375 Mass balance of the Antarctic Ice Sheet from 1992 to 2017, Nature, 558(7709), 219–222,
1376 doi:10.1038/s41586-018-0179-y, 2018a.

1377 Shepherd, A., Fricker, H. A. and Farrell, S. L.: Trends and connections across the Antarctic
1378 cryosphere, Nature, 558(7709), 223–232, doi:10.1038/s41586-018-0171-6, 2018b.

1379 Sherwood, S. C. and Huber, M.: An adaptability limit to climate change due to heat stress, Proc.
1380 Natl. Acad. Sci., 107(21), 9552, doi:10.1073/pnas.0913352107, 2010.

1381 Shi, J.-R., Xie, S.-P. and Talley, L. D.: Evolving Relative Importance of the Southern Ocean and
1382 North Atlantic in Anthropogenic Ocean Heat Uptake, J. Clim., 31(18), 7459–7479,
1383 doi:10.1175/JCLI-D-18-0170.1, 2018.

1384 Smith, D. M., Allan, R. P., Coward, A. C., Eade, R., Hyder, P., Liu, C., Loeb, N. G., Palmer, M.
1385 D., Roberts, C. D. and Scaife, A. A.: Earth's energy imbalance since 1960 in observations and
1386 CMIP5 models, Geophys. Res. Lett., 42(4), 1205–1213, doi:10.1002/2014GL062669, 2015.

https://doi.org/10.5194/essd-2019-255
Preprint. Discussion started: 20 March 2020
© Author(s) 2020. CC BY 4.0 License.

1387 Steiner, A., Ladstädter, F., Randel, W. J., Maycock, A. C., Claud, C., Fu, Q., Gleisner, H.,
1388 Haimberger, L., Ho, S.-P., Keckhut, P., Leblanc, T., Mears, C., Polvani, L., Santer, B., Schmidt,
1389 T., Sofieva, V., Wing, R. and Zou, C.-Z.: Observed temperature changes in the troposphere and
1390 stratosphere from 1979 to 2018, J. Clim., submitted, 2019.

1391 Stevens, C. W.: Subsurface investigation of shallow-water permafrost located within the near-
1392 shore zone of the Mackenzie Delta, Northwest Territories, Canada, University of Calgary., 2007.

1393 Stevens, M. B., González-Rouco, J. F. and Beltrami, H.: North American climate of the last
1394 millennium: Underground temperatures and model comparison, J. Geophys. Res. Earth Surf.,
1395 113(F1), doi:10.1029/2006JF000705, 2008.

1396 Stieglitz, M. and Smerdon, J. E.: Characterizing Land–Atmosphere Coupling and the
1397 Implications for Subsurface Thermodynamics, J. Clim., 20(1), 21–37, doi:10.1175/JCLI3982.1,
1398 2007.

1399 Storto, A., Masina, S., Simoncelli, S., Iovino, D., Cipollone, A., Drevillon, M., Drillet, Y.,
1400 Schuckman, K., Parent, L., Garric, G., Greiner, E., Desportes, C., Zuo, H., Balmaseda, M. and
1401 Peterson, K.: The added value of the multi-system spread information for ocean heat content and
1402 steric sea level investigations in the CMEMS GREP ensemble reanalysis product, Clim. Dyn.,
1403 doi:10.1007/s00382-018-4585-5, 2018.

1404 Straneo, F. and Cenedese, C.: The Dynamics of Greenland's Glacial Fjords and Their Role in
1405 Climate, Ann. Rev. Mar. Sci., 7(1), 89–112, doi:10.1146/annurev-marine-010213-135133, 2015.

1406 Straneo, F., Adusumilli, S., Slater, D., Timmermans, M. L., Marzeion, B. and Schweiger, A.:
1407 Increasing energy uptake by the melting cryosphere, in preparation, 2019a.

1408 Straneo, F., Sutherland, D. A., Stearns, L., Catania, G., Heimbach, P., Moon, T., Cape, M. R.,
1409 Laidre, K. L., Barber, D., Rysgaard, S., Mottram, R., Olsen, S., Hopwood, M. J. and Meire, L.:
1410 The Case for a Sustained Greenland Ice Sheet-Ocean Observing System (GrIOOS), Front. Mar.
1411 Sci., 6, 138 [online] Available from:
1412 https://www.frontiersin.org/article/10.3389/fmars.2019.00138, 2019b.

1413 Trenberth, K. E. and Fasullo, J. T.: Tracking Earth's Energy, Science (80-.)., 328(5976), 316,
1414 doi:10.1126/science.1187272, 2010.

1415 Trenberth, K. E., Fasullo, J. T. and Shepherd, T. G.: Attribution of climate extreme events, Nat.
1416 Clim. Chang., 5(8), 725–730, doi:10.1038/nclimate2657, 2015.

1417 Trenberth, K. E., Cheng, L., Jacobs, P., Zhang, Y. and Fasullo, J.: Hurricane Harvey Links to
1418 Ocean Heat Content and Climate Change Adaptation, Earth's Futur., 6(5), 730–744,
1419 doi:10.1029/2018EF000825, 2018.

1420 Vasseur, G., Bernard, P., Van de Meulebrouck, J., Kast, Y. and Jolivet, J.: Holocene
1421 paleotemperatures deduced from geothermal measurements, Palaeogeogr. Palaeoclimatol.
1422 Palaeoecol., 43(3–4), 237–259, doi:10.1016/0031-0182(83)90013-5, 1983.

https://doi.org/10.5194/essd-2019-255
Preprint. Discussion started: 20 March 2020
© Author(s) 2020. CC BY 4.0 License.

Watts, N., Amann, M., Arnell, N., Ayeb-Karlsson, S., Belesova, K., Boykoff, M., Byass, P., Cai, W., Campbell-Lendrum, D., Capstick, S., Chambers, J., Dalin, C., Daly, M., Dasandi, N., Davies, M., Drummond, P., Dubrow, R., Ebi, K. L., Eckelman, M., Ekins, P., Escobar, L. E., Fernandez Montoya, L., Georgeson, L., Graham, H., Haggar, P., Hamilton, I., Hartinger, S., Hess, J., Kelman, I., Kiesewetter, G., Kjellstrom, T., Kniveton, D., Lemke, B., Liu, Y., Lott, M., Lowe, R., Sewe, M. O., Martinez-Urtaza, J., Maslin, M., McAllister, L., McGushin, A., Jankin Mikhaylov, S., Milner, J., Moradi-Lakeh, M., Morrissey, K., Murray, K., Munzert, S., Nilsson, M., Neville, T., Oreszczyn, T., Owfi, F., Pearman, O., Pencheon, D., Phung, D., Pye, S., Quinn, R., Rabbaniha, M., Robinson, E., Rocklöv, J., Semenza, J. C., Sherman, J., Shumake-Guillemot, J., Tabatabaei, M., Taylor, J., Trinanes, J., Wilkinson, P., Costello, A., Gong, P. and Montgomery, H.: The 2019 report of The Lancet Countdown on health and climate change: ensuring that the health of a child born today is not defined by a changing climate, Lancet, 394(10211), 1836–1878, doi:10.1016/S0140-6736(19)32596-6, 2019.

WCRP, G. S. L. B.: Global sea-level budget 1993–present, Earth Syst. Sci. Data, 10(3), 1551–1590, doi:10.5194/essd-10-1551-2018, 2018.

Wijffels, S., Roemmich, D., Monselesan, D., Church, J. and Gilson, J.: Ocean temperatures chronicle the ongoing warming of Earth, Nat. Clim. Chang., 6(2), 116–118, doi:10.1038/nclimate2924, 2016.

Willis, J. K., Roemmich, D. and Cornuelle, B.: Interannual variability in upper ocean heat content, temperature, and thermosteric expansion on global scales, J. Geophys. Res. Ocean., 109(C12), doi:10.1029/2003JC002260, 2004.

Wilson, N., Straneo, F. and Heimbach, P.: Satellite-derived submarine melt rates and mass balance (2011–2015) for Greenland's largest remaining ice tongues, Cryosph., 11, 2773–2782, doi:10.5194/tc-11-2773-2017, 2017.

Woollings, T., Gregory, J. M., Pinto, J. G., Reyers, M. and Brayshaw, D. J.: Response of the North Atlantic storm track to climate change shaped by ocean–atmosphere coupling, Nat. Geosci., 5(5), 313–317, doi:10.1038/ngeo1438, 2012.

Xu, C., McDowell, N. G., Fisher, R. A., Wei, L., Sevanto, S., Christoffersen, B. O., Weng, E. and Middleton, R. S.: Increasing impacts of extreme droughts on vegetation productivity under climate change, Nat. Clim. Chang., 9(12), 948–953, doi:10.1038/s41558-019-0630-6, 2019.

Yang, H., Lohmann, G., Wei, W., Dima, M., Ionita, M. and Liu, J.: Intensification and poleward shift of subtropical western boundary currents in a warming climate, J. Geophys. Res. Ocean., 121(7), 4928–4945, doi:10.1002/2015JC011513, 2016.

Zanna, L., Khatiwala, S., Gregory, J. M., Ison, J. and Heimbach, P.: Global reconstruction of historical ocean heat storage and transport, Proc. Natl. Acad. Sci., 116(4), 1126, doi:10.1073/pnas.1808838115, 2019.

Zemp, M., Huss, M., Thibert, E., Eckert, N., McNabb, R., Huber, J., Barandun, M., Machguth, H., Nussbaumer, S. U., Gärtner-Roer, I., Thomson, L., Paul, F., Maussion, F., Kutuzov, S. and Cogley, J. G.: Global glacier mass changes and their contributions to sea-level rise from 1961 to

https://doi.org/10.5194/essd-2019-255
Preprint. Discussion started: 20 March 2020
© Author(s) 2020. CC BY 4.0 License.

2016, Nature, 568(7752), 382–386, doi:10.1038/s41586-019-1071-0, 2019.

Zhang, J. and Rothrock, D. A.: Modeling Global Sea Ice with a Thickness and Enthalpy Distribution Model in Generalized Curvilinear Coordinates, Mon. Weather Rev., 131(5), 845–861, doi:10.1175/1520-0493(2003)131<0845:MGSIWA>2.0.CO;2, 2003.

Zscheischler, J., Westra, S., van den Hurk, B. J. J. M., Seneviratne, S. I., Ward, P. J., Pitman, A., AghaKouchak, A., Bresch, D. N., Leonard, M., Wahl, T. and Zhang, X.: Future climate risk from compound events, Nat. Clim. Chang., 8(6), 469–477, doi:10.1038/s41558-018-0156-3, 2018.